Synthesis and evaluation of novel N1-acylated 5-(4-pyridinyl)indazole derivatives as potent and selective haspin inhibitors

Mona M. Shawky [a], Mennatallah Abdallah [a], Hend Khalifa [a], Youssef Aboushady [a], Ashraf H. Abadi [a], Matthias Engel [b,*], Mohammad Abdel-Halim [a,*]

[a] Department of Pharmaceutical Chemistry, Faculty of Pharmacy and Biotechnology, German University in Cairo, Cairo 11835, Egypt
[b] Pharmaceutical and Medicinal Chemistry, Saarland University, Campus C2.3, D-66123 Saarbrücken, Germany

ABSTRACT

Protein kinase dysregulation was strongly linked to cancer pathogenesis. Moreover, histone alterations were found to be among the most important post-translational modifications that could contribute to cancer growth and development. In this context, haspin, an atypical serine/threonine kinase, phosphorylates histone H3 at threonine-3 and is notably overexpressed in various common cancer types. Herein, we report novel 5-(4-pyridinyl)indazole derivatives as potent and selective haspin inhibitors. Amide coupling at *N*1 of the indazole ring with *m*-hydroxyphenyl acetic acid yielded compound **21** with an IC$_{50}$ value of 78 nM against haspin. This compound showed a meaningful selectivity over 15 of the most common off-targets, including Clk 1–3 and Dyrk1A, 1B, and 2. The most potent haspin inhibitors **5** and **21** effectively inhibited the growth of the NCI-60 cancer cell lines, further emphasizing the success of our scaffold as a new selective lead for the development of anti-cancer therapeutic agents.

1. Introduction

Protein kinases are well known for playing a crucial role in variable cellular pathways through catalyzing the phosphorylation process [1]. Dysregulation of protein kinases was linked to the pathogenesis of several diseases, including the development and growth of cancer cells [2]. In fact, cancer pathogenesis is now assumed to be linked not only with genetic alterations but also to changes in epigenetic mechanisms [3] and the alterations made to histone proteins are among the most significant post-translational modifications [4]. Haspin (haploid germ cell-specific protein kinase) is an atypical serine/threonine kinase which is encoded by Germ cell-specific gene 2 (*GSG2*) [5,6]. The haspin gene, *GSG2*, is also atypical since it is an intron-less gene [7] lying completely within the intron of the Integrin alpha E gene [8]. The significance of this protein is emphasized by the fact that there is at least one haspin homologue in most of the nearly complete sequenced eukaryotic genomes [9]. Haspin mRNA is expressed abundantly in testis but despite its name, haspin is not a germ cell-specific kinase. It is present as well in almost all proliferating cells in bone marrow, thymus, and fetal liver, and to a lesser extent in the lung, intestine, spleen, and in various other fetal tissues [10–12].

Haspin functions in the phosphorylation of histone H3 at threonine-3 (H3T3) during mitosis [13]. The resulting phospho-H3T3 is recognized by Survivin, a member of the chromosomal passenger complex (CPC), and this mediates the recruitment of the CPC to chromosomes [14–16]. The CPC, composed of Survivin, Aurora B, INCENP, and borealin, plays a critical role in regulating the processes of mitosis and cytokinesis [10]. After this recruitment, phospho-H3T3 functions as a docking site for the CPC at the centromere. This in turn activates Aurora B kinase which ensures appropriate kinetochore-microtubule attachment [17]. In addition, haspin is proposed to interact by its non-catalytic N terminus with Pds5B, a cohesion regulatory subunit [18], and with heterochromatin protein 1 (HP1) [19] where these interactions lead to haspin's localization at the centromeres phosphorylating Wapl at the YSR motif. Consequently, the Wapl-Pds5B interaction that normally would have led to the release of the cohesion complex from the centromeres is inhibited as a result of Wapl phosphorylation. Thus, it can be inferred that the interaction between haspin and Pds5B is crucial for maintaining proper cohesion of the sister chromatids [18,19]. Those functions were proven by the depletion of haspin by small interfering RNAs (siRNAs) which have resulted in misalignment of chromosomes in metaphase, premature loss of centromeric cohesion between sister chromatids, and eventually

mitotic arrest [5,11,17].

The regulation of haspin is proposed to require multiple key players. At the interphase, haspin is mainly autoinhibited by an autoinhibitory domain given the name Haspin Basic Inhibitory Segment or HBIS which folds on its catalytic domain inhibiting the enzyme's activity. This autoinhibition is neutralized by multiple phosphorylations of the enzyme's *N*-terminal domain by Cdk1 and Polo-like kinase 1 (Plk1) in the M phase [20,21]. Furthermore, it was found that haspin-mediated H3T3 phosphorylation requires the phosphorylation by Aurora B [22] as well as Aurora A enzymes [23].

Haspin is considered an attractive target since haspin inhibitors are proven to be potent antimitotic agents and they might have fewer side effects when compared to other anti-mitotic kinase targets [3]. Since haspin belongs to an atypical eukaryotic protein kinase family (aPKs) which is distinctly different from other conventional human kinases [24,25], haspin is characterized by a very unique binding site [6]. Not only the conserved ATP/Mg^{2+} binding motif Asp-Phe-Gly (DFG) found in other kinases is replaced by an Asp-Tyr-Thr (DYT) motif, but also the usually conserved Ala-Pro-Glu (APE) that is found at the activation segment is absent [5]. Because it works mainly on proliferating cells, it is expected that haspin inhibitors will not have a marked impact on non-proliferating cells [3]. In fact, haspin was found to be overexpressed in many of the most prevalent cancers including Burkitt's lymphoma and chronic lymphocytic leukemia [6], osteosarcoma [26], melanoma [27], non-small cell lung cancer [28], breast cancer [29], colorectal cancer [30], pancreatic ductal adenocarcinoma [31], gallbladder carcinoma [32], bladder cancer [33], cholangiocarcinoma [34], hepatocellular carcinoma [35], clear cell renal cell carcinoma [36], prostate cancer [37], and ovarian cancer [38] and it was further associated with poor prognosis including malignancy grade in some of them (Supporting Information, Table S1).

Even though haspin has shown great potential as anticancer drug target, few potent inhibitors having different scaffolds were reported. For instance, 5-iodotubercidin (5-Itu) (**1**) is a nucleoside derivative which was commonly used as a potent haspin inhibitor (Fig. 1), however, many anti-cancer cellular effects of 5-Itu were attributed to off-targets inhibition and its genotoxic effects [12]. It showed marked cross-reactivity with members of the CMGC kinase family including Clk2 and Dyrk1A and Dyrk2 enzymes [39]. Furthermore, acridine analogues LDN-192960 (**2**) and LDN-209929 (**3**) were proposed to have potent scaffold for haspin inhibition. The poor selectivity of LDN-192960 (**2**) against Clk1, Dyrk1A, Dyrk2 and Dyrk3 has led to further optimization of the scaffold yielding LDN-209929 (**3**). Although this optimization enhanced the compound's selectivity towards haspin over Dyrk2, further information about its selectivity against other common off-targets was not provided [13]. Another scaffold was identified as a possible hit for haspin inhibition which was the β-carboline scaffold

yielding compound LDN-211898 (**4**). This compound has shown promising haspin inhibition, but lacked selectivity against other kinases including Clk1, Clk2, Dyrk1A, Dyrk1B, and Dyrk3 [40]. Several other scaffolds were proposed including pyridoquinazoline-based inhibitors [41], substituted 5,7-dihydro-6*H*-indolo[2,3-*c*]quinolin-6-one derivatives [42], 7-azaindole derivatives [43], 3*H*-pyrazolo[4,3-*f*]quinoline derivatives [4], and bisubstrate-analogue inhibitors [44]. Despite the fact that these scaffolds have demonstrated promising inhibitory effects on haspin, the primary challenge that persists is achieving selectivity over other kinases. Another commonly used haspin inhibitor is CHR-6494 (**5**) having an imidazopyridazine scaffold and it is considered as one of the most potent inhibitors [3]. However, it seems that CHR-6494 selectivity is questionable since it was not selective against Clk1 and Dyrk1A and its selectivity against Clk2–4 and Dyrk1B was not reported. In fact, as we have witnessed in most of the inhibitors, the most challenging off-targets opposing the selectivity of haspin inhibitors were found to be mainly Clk and Dyrk families. This is most likely attributable to the presence of a common hydrophobic bulky residue located *N*-terminal to the DFG motif (in haspin DYT) in those kinases. This creates a tight back pocket, stabilizing unique binding modes by anchoring inhibitors between the gatekeeper and this large hydrophobic residue [41,45].

This study presents the synthesis of new 5-(4-pyridinyl)indazole derivatives, which are effective haspin inhibitors exhibiting remarkable selectivity against many common off-targets. Some of these derivatives have shown anticancer properties against various NCI-60 cancer cell lines.

2. Results and discussion

2.1. Compound design

Our developed series is based on compound **MYF42** (Fig. 1), an unpublished hit compound having a *N*1-acylated 5-pyridin-4-yl-1*H*-indazol-3-yl amine scaffold discovered by our research group. This compound was identified as a potential lead for the development of selective haspin inhibitors with IC$_{50}$ of 240 nM at 25 μM ATP. Selectivity screening vs. several related kinases was done and **MYF42** showed the highest activity against haspin followed by Clk4 (Supporting Information, Table S2). It is worth mentioning that the indazole is considered as a "Privileged Scaffold" with more than 40 indazole-based therapeutic agents are already being used in clinical applications or still at clinical trials against various biological targets [46]. Hence, our diversification strategy aimed at fixing the indazole ring while performing structural modifications by replacing the 4-pyridinyl ring with a 3-pyridinyl to verify the optimum position of the pyridine nitrogen, and modifying the *N*1-phenacyl side chain by: monosubstitution at various positions of the phenyl ring using different electron-withdrawing and donating groups, replacing the phenyl ring with bicyclic rings or extending the spacer length.

2.2. Chemistry

The synthesis of 1-[3-amino-5-(pyridin-3/4-yl)-1*H*-indazol-1-yl] ethan-1-one derivatives was afforded through a two-step synthesis (Scheme 1). The synthesis started with a Palladium-Catalyzed Suzuki-Miyaura cross-coupling reaction between 5-bromo-1*H*-indazol-3-amine and pyridin-3-yl boronic acid using cesium carbonate as a base to yield 5-(pyridin-3-yl)-1*H*-indazol-3-amine (**A**) in a good yield. Compound **A** was further coupled with phenyl acetic acid in the presence of EDC as a coupling agent and DMAP to get compound **1** with good yield.

In the same manner, to synthesize the 5-(4-pyridinyl) derivatives, 5-bromo-1*H*-indazol-3-amine and pyridin-4-yl boronic acid were coupled using the same conditions as above to yield 5-(pyridin-4-yl)-1*H*-indazol-3-amine (**B**) which was further allowed to perform amide coupling with the appropriate acetic acid derivatives to yield compounds (**2–25**) in a
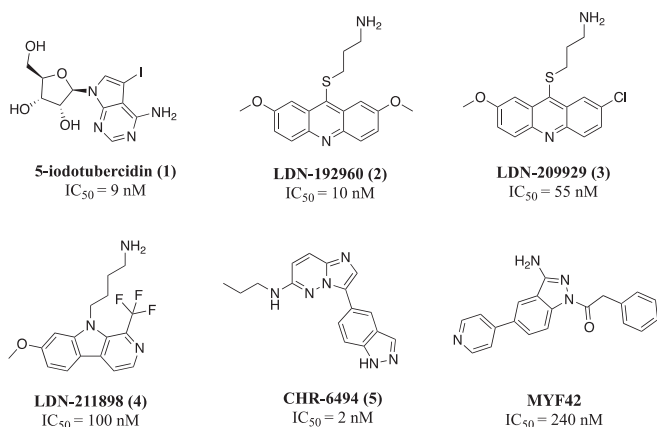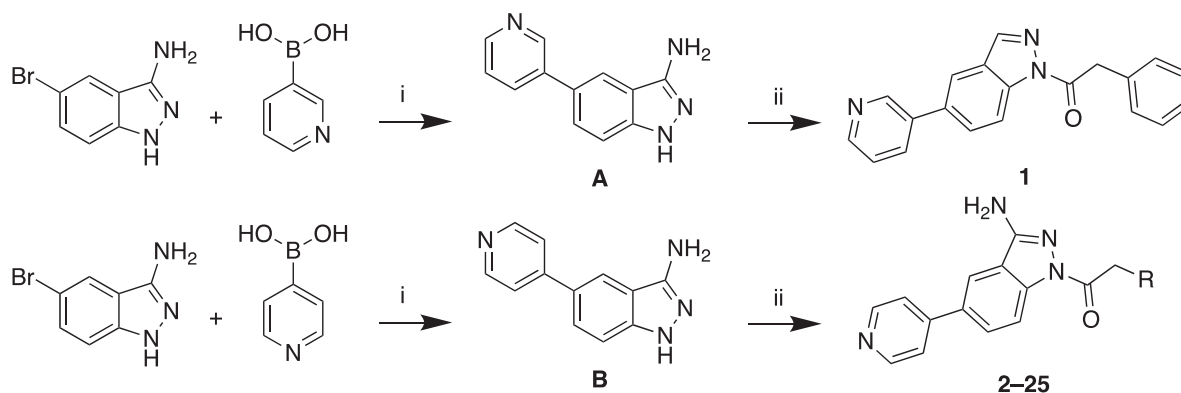

Fig. 1. Examples of reported haspin inhibitors and the hit compound **MYF42** (**this work**) together with their IC$_{50}$ values for haspin.

Below the figure, structures are labeled:

5-iodotubercidin (1)
IC$_{50}$ = 9 nM

LDN-192960 (2)
IC$_{50}$ = 10 nM

LDN-209929 (3)
IC$_{50}$ = 55 nM

LDN-211898 (4)
IC$_{50}$ = 100 nM

CHR-6494 (5)
IC$_{50}$ = 2 nM

MYF42
IC$_{50}$ = 240 nM

Scheme 1. Synthesis of compounds (**1**–**25**). Reagents and conditions: (i) 4 equiv of the pyridine boronic acid, 4 equiv of Cs_2CO_3, 0.1 equiv of [Pd(dppf)Cl$_2$] in 1,4-dioxane: water(4:1), reflux overnight (ii) 2 equiv of the appropriate acetic acid derivative, 2 equiv of EDC, 2 equiv of DMAP in DCM, stirring, rt, overnight.

Cpd no.	R	Cpd no.	R	Cpd no.	R
2	2-fluorophenyl	10	4-bromophenyl	18	2-methoxyphenyl
3	3-fluorophenyl	11	2-trifluoromethylphenyl	19	3-methoxyphenyl
4	4-fluorophenyl	12	3-trifluoromethylphenyl	20	4-methoxyphenyl
5	2-chlorophenyl	13	4-trifluoromethylphenyl	21	3-hydroxyphenyl
6	3-chlorophenyl	14	2-nitrophenyl	22	4-hydroxyphenyl
7	4-chlorophenyl	15	3-nitrophenyl	23	2-(napthalen-2-yl)
8	2-bromophenyl	16	2-methylphenyl	24	2,2-diphenyl
9	3-bromophenyl	17	4-methylphenyl	25	phenoxy

30–40 % yield.

2.3. Biological evaluation

2.3.1. SAR for haspin inhibition

The *in vitro* inhibitory activity of the novel indazole derivatives was assessed against haspin at a screening dose of 1 μM and the IC$_{50}$ values were determined for compounds exhibiting more than 60 % inhibition at 25 μM ATP (Table 1). Since **MYF42** has shown activity against Clk4 and because it is one of the common haspin off-targets, all of the final compounds were tested against Clk4 in parallel to obtain a primary indication of selectivity.

For haspin inhibition, the following structure–activity relationship (summarized in Fig. 2) can be concluded:

Shifting the nitrogen in the 4-pyridyl ring (compound 1). Replacing the 4-pyridinyl ring with a 3-pyridinyl ring (**1**) resulted in a decrease in the potency towards haspin inhibition. Therefore, the goal to synthesize potent haspin inhibitors was seen to be more achievable by performing modifications on the 4-pyridinyl rather than the 3-pyridinyl scaffold.

Optimization by various substitution patterns on the phenyl ring:

i) Mono substitution by electron-withdrawing groups (EWG). The substitution of the phenyl ring with *ortho* fluoro (**2**, IC$_{50}$ = 260 nM) was shown to be equipotent to the unsubstituted phenyl in **MYF42**. However, substitution with *meta*- (**3**) or *para*- (**4**) fluoro substituents resulted in reduced activity against haspin. Furthermore, *o*-chlorophenyl (**5**) and *o*-bromophenyl (**8**) derivatives showed a marked improvement of potency against haspin with IC$_{50}$ = 130 nM and 150 nM respectively. Likewise, *meta*- and *para*-chloro and bromo phenyl derivatives showed a decrease in the inhibitory potency with % inhibition below 40 % at 1 μM. Replacing halogens with the trifluoromethyl has markedly decreased the inhibitory activity with the *ortho* position (**11**)

showed the best activity with 49 % inhibition at 1 μM followed by *meta* then *para* analogues. Substitution by the more polar stronger EWG (the nitro group) significantly reduced the potency. To conclude, *ortho* substitution showed marked improvement in activity compared to the *meta* and *para* in all EWG. Since *o*-halogenated phenyl derivatives showed an enhancement in their potency when compared with the *meta* and *para* derivatives, and other *ortho* electron-withdrawing groups, this suggests that this *ortho* substitution stabilizes the biologically active conformation or it makes lipophilic interactions, or both.

ii) Mono substitution by electron-donating groups (EDG). Introducing a methyl group at the *ortho* (**16**) or *para* (**17**) position resulted in reduced inhibitory activity. However, it maintained the previously observed trend where *ortho* substitution exhibited better activity than *para* substitution, with a 53 % inhibition at 1 μM. Replacing the alkyl group with a stronger EDG (a methoxy group) further reduced the potency at all the tried positions (compounds **18**–**20**). Substitution of the phenyl ring with a hydroxyl group has shown a marked enhancement of potency. The *meta*-hydroxyphenyl derivative (**21**, IC$_{50}$ = 78 nM) emerged as the most potent compound against haspin and showed more than double the potency of the *para*-hydroxyphenyl derivative (**22**, IC$_{50}$ = 160 nM). The hydroxyl group can be presumably involved in a potential H-bonding interaction (see the docking section).

In general, compounds featuring methyl and methoxy groups as substituents exhibited lower activity compared to their halogen counterparts. The *para* position showed low tolerance to various substituents, with the exception of the hydroxyl group. Utilizing the hydroxyl group at the *meta* or *para* positions led to an increase in potency, indicating that hydrogen bonding, particularly with the *meta* hydroxyl group, plays a significant role in the interaction with the active site.

Using extended aromatic systems. The effect of replacing the phenyl ring in **MYF42** with other aromatic rings was examined by substituting the phenyl with either 2-naphthyl (**23**) or adding an additional phenyl (benzhydryl in **24**). Both modifications showed a
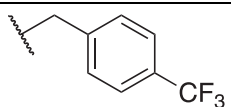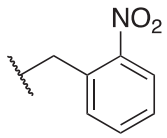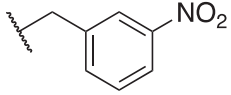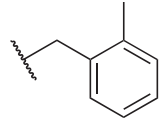
Table 1

Inhibition of haspin and Clk4 by compounds **1–25**.
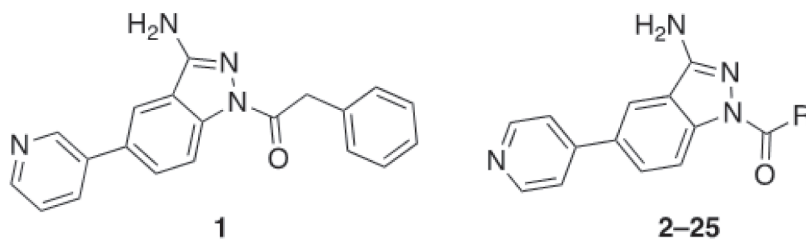
Compound No.	R	Haspin %Inhibition	IC$_{50}$	Clk4 %Inhibition	IC$_{50}$
		At 1 μM[a]	(nM)	At 1 μM[a]	(nM)
1	–	41 ± 1.0	n.d.	34 ± 1.0	n.d.
2		87 ± 0.5	260 ± 3.3	31 ± 0.5	n.d.
3		49 ± 0.5	n.d.	32 ± 1.0	n.d.
4		43 ± 1.0	n.d.	19 ± 1.5	n.d.
5		88 ± 2.9	130 ± 2.2	39 ± 0.5	n.d.
6		38 ± 3.0	n.d.	49 ± 0.5	n.d.
7		30 ± 2.5	n.d.	18 ± 2.0	n.d.
8		87 ± 1.0	150 ± 1.4	42 ± 0.0	n.d.
9		17 ± 3.0	n.d.	38 ± 0.5	n.d.
10		29 ± 3.5	n.d.	72 ± 2.3	390 ± 3.8
11		49 ± 1.0	n.d.	14 ± 1.5	n.d.
12		ni	n.d.	16 ± 2.0	n.d.

4

Table 1 (*continued*)

Compound No.	R	Haspin %Inhibition At 1 µM[a]	IC$_{50}$ (nM)	Clk4 %Inhibition At 1 µM[a]	IC$_{50}$ (nM)
13		ni	n.d.	3 ± 1.0	n.d.
14		34 ± 0.5	n.d.	48 ± 2.5	n.d.
15		9 ± 1.5	n.d.	22 ± 1.0	n.d.
16		53 ± 4.5	n.d.	27 ± 2.0	n.d.
17		27 ± 0.5	n.d.	30 ± 0.5	n.d.
18		20 ± 1.0	n.d.	16 ± 0.5	n.d.
19		22 ± 0.5	n.d.	6 ± 1.5	n.d.
20		30 ± 1.5	n.d.	18 ± 1.0	n.d.
21		93 ± 1.5	78 ± 2.5	73 ± 2.5	360 ± 3.6
22		86 ± 2.0	160 ± 1.6	36 ± 1.0	n.d.
23		0 ± 1.0	n.d.	12 ± 0.0	n.d.
24		ni	n.d.	ni	n.d.
25		68 ± 1.5	460 ± 2.4	82 ± 1.0	230 ± 1.3
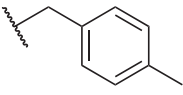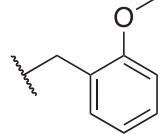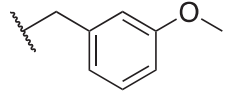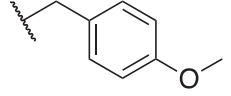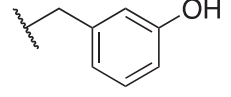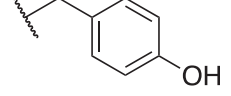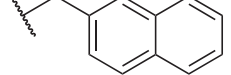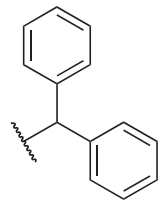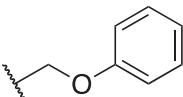
[a] Data shown is the mean of at least two independent experiments, values are mean +/- SEM. n.d., not determined. ni, no inhibition.

Fig. 2. Summary of the SAR for compounds having activity against haspin.

deterioration in the inhibitory activity against haspin. Therefore, the presence of the less bulky phenyl ring appears necessary for enhancing the potency.
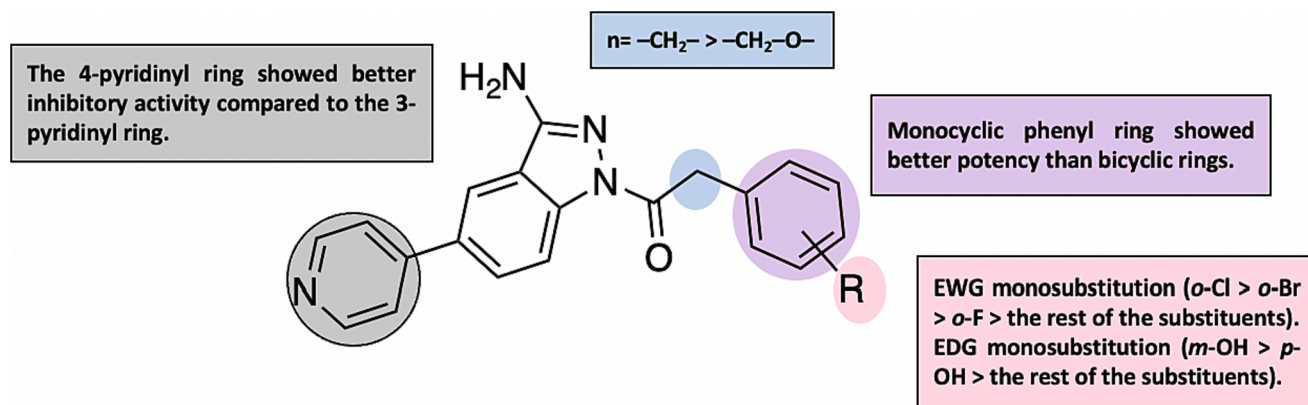
Insertion of oxygen in the spacer. Finally, increasing the spacer length by including an oxygen atom resulted in a two-fold decrease in the inhibitory activity as elicited by the phenoxy acetyl derivative (**25**).

Clk4 inhibition. Most of the compounds weakly inhibited Clk4 with less than 50 % at 1 μM (Table 1) and hence there was no improvement of potency when compared to **MYF42** (unsubstituted phenyl derivative). However, the following modifications have shown an improvement in potency against Clk4 including: 1) substitution with a *para*-bromo group on the phenyl ring (compound **10**, IC$_{50}$ = 390 nM), this compound showed selective inhibition for Clk4 vs haspin, 2) substitution with *meta*-hydroxyl group on the phenyl ring (compound **21**, IC$_{50}$ = 360 nM), this compound was about 5-fold more potent towards haspin, 3) increasing the spacer length from one to two atoms by including an oxygen atom which resulted in a marked increase in Clk4 inhibitory potency (compound **25**, IC$_{50}$ = 230 nM), this compound also inhibited haspin but with 2-fold lower potency.

2.3.2. Extended kinase selectivity profiling

The most potent haspin inhibitor, compound **21**, was additionally tested against a panel of kinases that were reported to be the major haspin off-targets at 1 μM (Table 2) [12,42,43,47].

From the selectivity screening results, we can observe that compound **21** has shown a characteristic selectivity against 14 of the most common off-targets. It was markedly selective against Clk (1–3) and Dyrk (1A, 1B, and 2) isoforms. Its major off-target is Clk4, however, the selectivity index (SI) calculated as IC$_{50}$ Clk4 /IC$_{50}$ haspin is equal to 4.6 towards haspin than Clk4. Interestingly, the compound did not cross-

react with Clk1 despite the high homology between Clk4 and Clk1 [48]. In conclusion, compound **21** has successfully overcome the selectivity problems against Clk and Dyrk isoforms that were found in CHR-6494 and other reported inhibitors mentioned before.

2.3.3. Single-dose profiling against NCI-60 cancerous cell lines

Because of the postulated involvement of haspin in cancer pathogenesis, the most potent haspin inhibitors in our series were investigated for their potential as anticancer agents. *In vitro* anticancer activity screening was done for five compounds along with **MYF-42** at the Developmental Therapeutics Program (DTP) of the National Cancer Institute (NCI) utilizing a panel of 60 human tumor cell lines originating from 9 tissue types [49]. Submitted compounds are subjected to a single-dose screening (10^{-5} M) in the full NCI-60 panel. The outcome of this assay is the measured percent growth for each treated cell and a mean graph is provided (Supporting information, Figs. S1–S6). This allowed the detection of both growth inhibition (by subtracting the value of the growth percent from 100 %) and lethality with growth % values less than 0. The % growth inhibition measured against all 60 cell lines along with the mean growth inhibition % for compounds **2**, **5**, **8**, **21**, **22**, and the lead compound **MYF42** are provided in Table 3.

As discussed earlier, haspin overexpression can be expected in almost all cancer cell types. Indeed, compound **5** showed activity against diverse cancer cell lines from different tissue origins, most strongly against HS 578T breast cancer cell, HOP-92 non-small cell lung cancer, and RXF 393 renal cancer cell lines. Compound **5** was shown to be the most potent inhibitor against the whole panel of cell lines which could be contributed to factors like cell membrane permeability and serum protein binding in the medium which influences the overall potency of a given compound. It is worth mentioning that triple-negative breast cancers (TNBCs) are a challenging type of cancer characterized by poor prognosis and the lack of treatment options since it lacks estrogen and progesterone receptors and there is no HER2 overexpression [50] and luckily, some of the tested compounds have shown marked % inhibition against it including compound **2** against HS 578T cell lines, compound **5** against HS 578T, BT-549, and MDA-MB-468 cell lines, and compound **21** showed activity towards HS 578T and BT-549 cell lines. It is worth mentioning that testing the compounds against a broader kinome panel will be beneficial to conclude that these effects are specifically related to haspin inhibition.

2.4. In silico examinations

2.4.1. Molecular docking

To gain a more comprehensive understanding of the binding mode of compound **21**, the most potent haspin inhibitor (IC$_{50}$ haspin = 78 nM), molecular docking was performed at haspin's ATP binding pocket (PDB code: 7OPS) using MOE (Fig. 3). The hypothetical binding model

Table 2
Selectivity profiling of compound **21**.

Kinase	% Inhibition at 1 μM	IC$_{50}$
Haspin	95	78
CDK5/p25	16	n.d.
Clk1	9	n.d.
Clk2	29	n.d.
Clk3	9	n.d.
Clk4	69	360
CSNK1D (CK1 delta)	8	n.d.
CSNK2A1 (CK2 alpha 1)	10	n.d.
Dyrk1A	8	n.d.
Dyrk1B	8	n.d
Dyrk2	24	n.d.
HIPK1 (Myak)	3	n.d.
NTRK2 (TRKB)	0	n.d.
PIM1	6	n.d.
SRPK1	8	n.d.
STK17A (DRAK1)	17	n.d.

Table 3
Growth inhibition % for each cell line in all panels for compounds (**2**, **5**, **8**, **21**, **22**, and **MYF42**) at 10^{-5} M.*

Panel	Cell line	Growth inhibition %					
		Compound					
		2	**5**	**8**	**21**	**22**	**MYF42**
Leukemia	CCRF-CEM	37.15	59.11	—	47.27	13.81	5.23
	HL-60(TB)	66.91	72.27	22.68	25.69	40.34	39.21
	K-562	32.90	74.21	11.14	13.01	6.97	22.89
	MOLT-4	41.82	68.1	13.18	13.36	10.38	22.04
	RPMI-8226	49.37	71.61	—	10.44	—	22.28
	SR	63.58	76.95	29.42	54.83	14.13	61.8
Non-small cell lung cancer	A549/ATCC	17.18	57.09	4.81	2.26	1.28	27.18
	EKVX	80.61	90.00	45.57	59.48	28.06	39.90
	HOP-62	47.45	36.59	12.85	32.36	7.53	20.00
	HOP-92	113.18	105.12	51.58	54.74	62.96	42.34
	NCI-H226	57.97	63.05	27.76	1.14	8.44	13.30
	NCI-H23	22.60	40.03	10.26	12.90	7.01	27.18
	NCI-H460	13.38	43.25	—	9.44	0.01	11.92
	NCI-H522	49.09	73.81	29.61	59.97	19.63	27.10
Colon cancer	COLO 205	1.57	42.85	—	—	—	—
	HCC-2998	3.19	27.71	—	—	—	—
	HCT-116	29.44	59.08	9.09	12.42	0.43	13.89
	HCT-15	29.66	59.41	5.95	—	1.54	23.44
	HT29	15.64	64.60	—	—	—	13.04
	KM12	6.36	30.79	—	—	—	7.08
	SW-620	3.05	34.69	—	24.35	—	—
CNS cancer	SF-268	36.02	40.25	1.71	40.57	15.99	31.04
	SF-295	47.00	75.43	16.63	25.16	7.09	20.99
	SF-539	50.08	60.80	15.29	34.91	20.88	48.28
	SNB-19	21.73	47.47	4.11	5.85	0.31	15.47
	SNB-75	41.15	75.26	33.15	68.45	49.19	86.62
	U251	—	42.15	—	—	—	19.61
Melanoma	LOX IMVI	32.45	53.46	—	7.79	—	21.96
	MALME-3M	24.52	41.73	18.23	12.29	10.08	17.7

Table 3 (*continued*)

Panel	Cell line	Growth inhibition %					
		Compound					
		2	**5**	**8**	**21**	**22**	**MYF42**
Leukemia	CCRF-CEM	37.15	59.11	—	47.27	13.81	5.23
	HL-60(TB)	66.91	72.27	22.68	25.69	40.34	39.21
	K-562	32.90	74.21	11.14	13.01	6.97	22.89
	MOLT-4	41.82	68.1	13.18	13.36	10.38	22.04
	RPMI-8226	49.37	71.61	—	10.44	—	22.28
	SR	63.58	76.95	29.42	54.83	14.13	61.8
Non-small cell lung cancer	A549/ATCC	17.18	57.09	4.81	2.26	1.28	27.18
	EKVX	80.61	90.00	45.57	59.48	28.06	39.90
	HOP-62	47.45	36.59	12.85	32.36	7.53	20.00
	HOP-92	113.18	105.12	51.58	54.74	62.96	42.34
	NCI-H226	57.97	63.05	27.76	1.14	8.44	13.30
	NCI-H23	22.60	40.03	10.26	12.90	7.01	27.18
	NCI-H460	13.38	43.25	—	9.44	0.01	11.92
	NCI-H522	49.09	73.81	29.61	59.97	19.63	27.10
Colon cancer	COLO 205	1.57	42.85	—	—	—	—
	HCC-2998	3.19	27.71	—	—	—	—
	HCT-116	29.44	59.08	9.09	12.42	0.43	13.89
	HCT-15	29.66	59.41	5.95	—	1.54	23.44
	HT29	15.64	64.60	—	—	—	13.04
	KM12	6.36	30.79	—	—	—	7.08
	SW-620	3.05	34.69	—	24.35	—	—
CNS cancer	SF-268	36.02	40.25	1.71	40.57	15.99	31.04
	SF-295	47.00	75.43	16.63	25.16	7.09	20.99
	SF-539	50.08	60.80	15.29	34.91	20.88	48.28
	SNB-19	21.73	47.47	4.11	5.85	0.31	15.47
	SNB-75	41.15	75.26	33.15	68.45	49.19	86.62
	U251	—	42.15	—	—	—	19.61
Melanoma	LOX IMVI	32.45	53.46	—	7.79	—	21.96
	MALME-3M	24.52	41.73	18.23	12.29	10.08	17.7

Table 3 (*continued*)

Mean growth inhibition %		30.53	54.68	10.07	17.00	7.15	22.00
IC$_{50}$ vs. Haspin (nM)		260	130	150	78	160	240
Color Scale:	-20 Minimum inhibition		17 Median			120 Maximum inhibition	

*Table entries are highlighted according to the value of % growth inhibition. Blank entries (-) indicate no growth inhibition observed, but rather a growth-inducing activity was observed, i.e., a negative value of % GI.

revealed anchoring of compound **21** in the binding pocket by: i) two CH-π interactions that were found between the pyrazole ring of the indazole and Ile490, and between the pyridine ring and Val498. ii) several H-bond interactions which are recognized between *N* of the pyridine ring acting as HBA and the conserved Lys511, and between the proton of the amino group (HBD) and the carbonyl group present at Gly609 at the hinge region. Importantly, a charge-supported H-bond interaction is prominent between the phenolic OH group and Glu613, and this critical interaction could contribute to the improved potency of compound **21** among the synthesized series. It should be noted that the hydroxybenzyl extension of **21** protrudes beyond the ATP binding pocket of haspin (Fig. 3B) to reach the non-conserved residue Glu613 outside the pocket. This interaction cannot occur with closely related off-target kinases as they do not possess a glutamic acid or a homologous residue at that position. Given that the unsubstituted congener **1** only provides a moderate, basal activity against haspin (Table 1), the additional charge-supported H-bond enabled by the 3-hydroxy substituent critically enhanced the potency and selectivity towards haspin.

2.4.2. Calculated physicochemical and pharmacokinetic properties

Compounds **5** and **21**, the most potent against haspin, were evaluated *in silico* for their physicochemical and drug-like properties using the SWISS-ADME online platform. The compounds' molecular weights did not exceed 500, their XlogP3 values were < 5, the number of hydrogen bond acceptors (HBA) in the two compounds was ≤ 10, and the number of hydrogen bond donors (HBD) was ≤ 5. Therefore, both compounds were shown to obey Lipinski's rule of five without any violations and accordingly, this indicates their potential as orally bioavailable drugs as shown in Table 4. The two compounds are predicted to be moderately soluble because their logS value lies between − 6 and − 4. Moreover, the topological polar surface area (TPSA), which is the polarity estimate, of both compounds lie between the optimum range of 20–130 Å^2.

For prediction of the passive human gastrointestinal absorption and brain access of both the tested molecules, the BOILED-Egg (Brain Or IntestinaL EstimateD permeation predictive model) plot of the cLogP method developed by Wildman and Crippen (WLOGP) versus topological polar surface area (TPSA) was retrieved from the Swiss-ADME
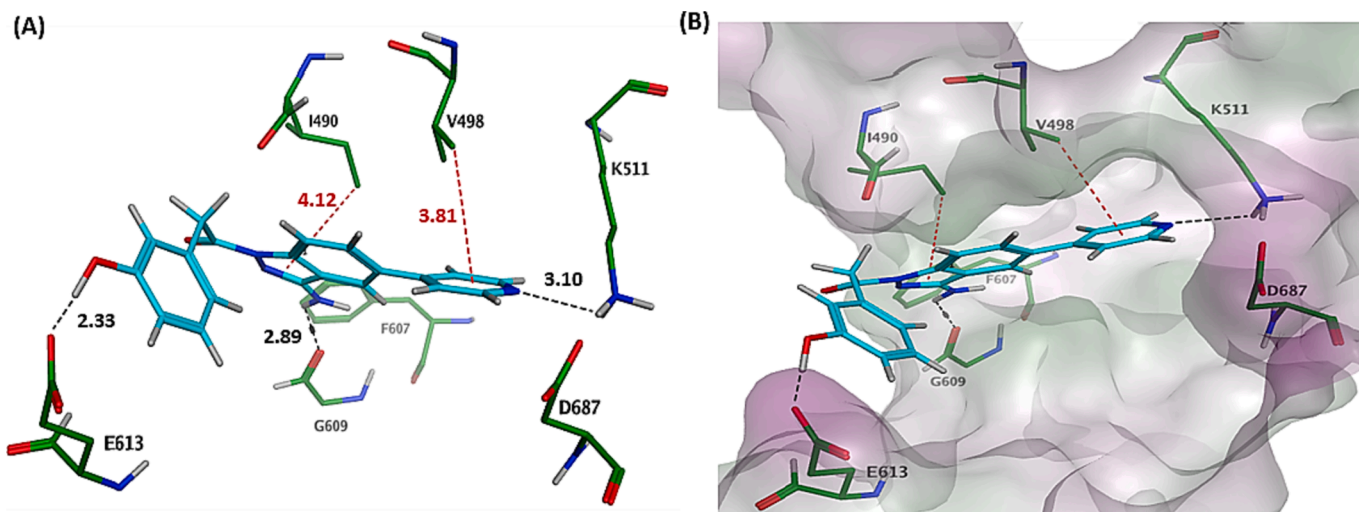

Fig. 3. Hypothetical binding model for the interaction between compound **21** and the ATP binding pocket of haspin (PDB code: 7OPS). **21** (cyan blue) was docked into the ATP pocket of haspin using MOE. (A) In the binding model, **21** is anchored through two CH-π interactions between the pyrazole and pyridine rings with Ile490 and Val498 respectively. Moreover, H bonds are prominent between the *N* of the pyridine ring and the conserved Lys511, as well as between the amino group and Gly609 at the hinge region. In addition, a charge-supported H-bond interaction is predicted between the phenolic OH group and Glu613. (B) Rotated view showing compound **21** in haspin's ATP binding pocket. Residues that interact directly or indirectly with the ligand are labelled while some residues in the front were omitted for clarity. Interactions are indicated by dashed lines and distances between the heavy atoms are given in Å (Dark red; CH-π interactions, Black; Hydrogen bonds). In the color code of the ATP binding pocket surface, the most lipophilic areas are indicated in green, while the most hydrophilic areas in magenta. (For interpretation of the references to color in this figure legend, the reader is referred to the web version of this article.)

Table 4
Molecular Properties and Drug-Likeness of the most potent candidates.[a]

Compound	HBA	HBD	M.Wt. (g/mol)	*n* rotb	MR	Log S	TPSA (A²)	XlogP3	Drug likeness (*Lipinski/ Pfizer filter*)
5	3	1	362.81	4	103.36	−4.87	73.80	3.88	"yes, a drug like" $M_w \leq 500$, Log p ≤ 5, HBA ≤ 10, and HBD ≤ 5
21	4	2	344.37	4	100.37	−4.14	94.03	2.90	

[a] HBA: the number of hydrogen bond acceptors, HBD: the number of hydrogen bond donors, M.Wt.: molecular weight, n rotb: number of rotatable bonds, MR: molar refractivity, Log S: solubility estimate, TPSA: topological polar surface area, and XlogP3: lipophilicity estimate.

platform (Fig. 4) [51]. The blue dots are indicating that these molecules are predicted to be effluxed by P-glycoproteins while the red one is indicating that this compound is predicted to not act as a substrate for P-glycoproteins. Both compounds are predicted to have good human intestinal absorption since they lie within the white area of the egg. Compound **5** appears to be capable of permeating the blood–brain barrier (BBB), as indicated by its location within the "yellow egg yolk" region. Additionally, it is predicted not to be expelled by P-glycoprotein (P-gp). Given its demonstrated effectiveness against various CNS cancer cell lines in the NCI-60 panel, compound **5** might be tested further in PK studies to verify CNS penetration and eventually in brain tumor models [52].

3. Conclusion

The current work presented a novel series of 1-[3-amino-5-(pyridin-4-yl)-1*H*-indazol-1-yl]ethan-1-one derivatives as potent and selective inhibitors of haspin. Among all employed structural modifications, the introduction of *m*-hydroxyphenyl acetyl group to *N*1 of the indazole ring has yielded compound **21**, the most potent haspin inhibitor in the series, with an IC$_{50}$ value of 78 nM. This compound exhibited exceptional

selectivity over the most common off-targets including Dyrk and Clks, with Clk4 being the most affected off-target with almost 5 times lower potency when compared to haspin. Therefore, compound **21** can be considered as a lead compound for the development of selective haspin inhibitors. On the other hand, analogs of **21** showing almost equal co-inhibition of Clk4, such as compound **25,** might also be useful as tools for studying potential synergistic effects due to inhibition of both targets. Such dual haspin/Clk4 inhibitors were not described yet and could become more interesting once the knowledge on the role of Clk4 in cancer pathogenesis increases [53,54]. Moreover, compounds **2, 5** and **21** have demonstrated marked inhibitory activity against several NCI cancer cell lines, further underlining the potential effectiveness of this scaffold as an anti-cancer agent.

4. Experimental section

4.1. Chemistry

Solvents and reagents were procured from commercial suppliers and utilized as received. All starting materials were sourced from Sigma-Aldrich and Chem PUR without purification. Intermediates and
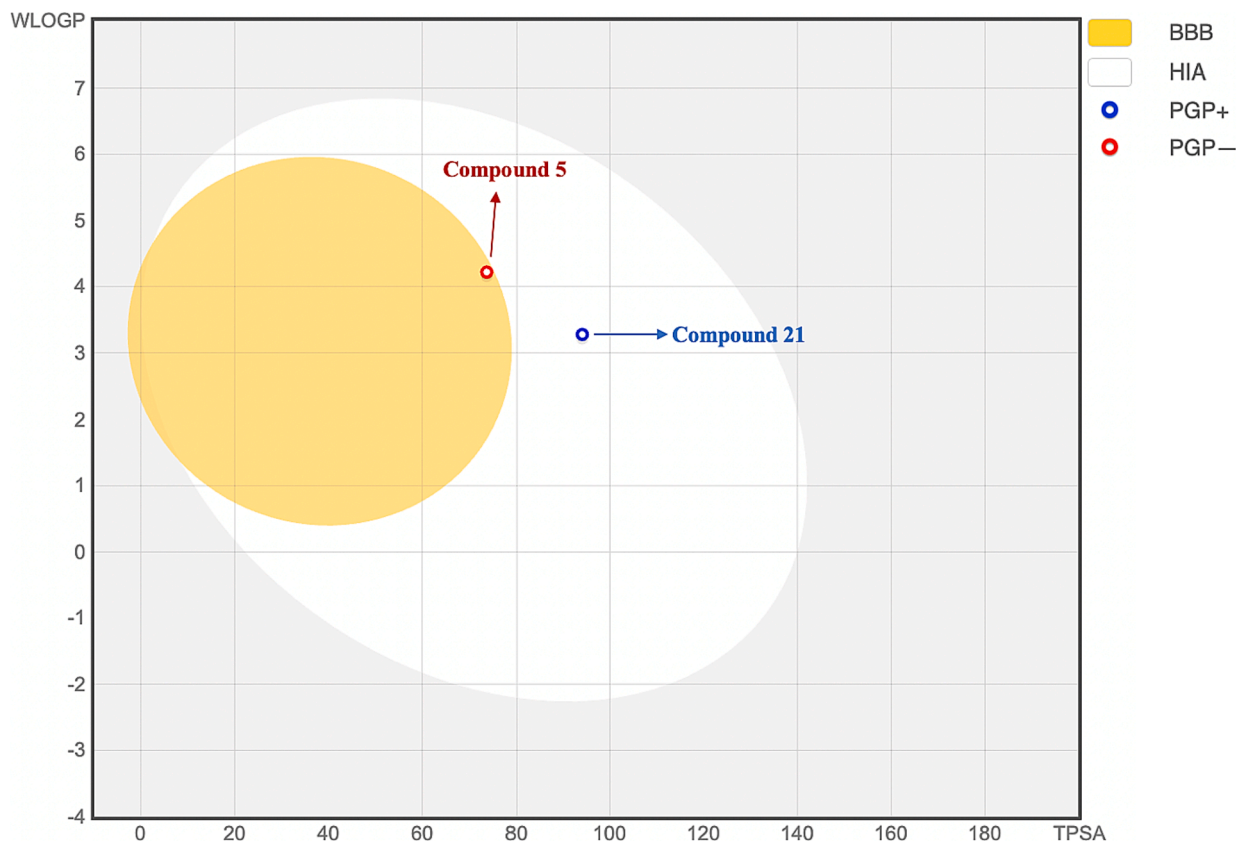

Fig. 4. BOILED-Egg representation for the predicted BBB penetration (egg-yolk area), and human intestinal absorption (egg area) of synthesized molecules (small red and blue circles). (For interpretation of the references to color in this figure legend, the reader is referred to the web version of this article.)

products were purified through column chromatography using silica gel 60 (40–63 μM). The reaction progress was monitored by TLC with fluorescent pre-coated silica gel plates, and components' detection was performed under short UV light (λ = 254 nm). ^{1}H NMR and ^{13}C NMR spectra were obtained by a Bruker DRX 500 spectrometer or a Varian 400 spectrometer using deuterated DMSO (DMSO-d_6) as NMR solvent. Chemical shifts (δ) were expressed in parts per million (ppm) and referenced to the residual solvent signals (DMSO-d_6: 2.50 and 39.52 ppm for ^{1}H and ^{13}C, respectively). Analysis of all spectra was conducted using MestReNova software, version 6.0.2–5475. All final compounds had shown a purity percentage of at least 95 % determined by UHPLC coupled with a mass spectrophotometer. Mass spectrometric analysis (UHPLC-ESI-MS) was performed using Waters ACQUITY Xevo TQD system. This system comprises an ACQUITY UPLC H-Class system and Xevo™ TQD triple-quadrupole tandem mass spectrometer with an electrospray ionization (ESI) interface (Waters Corp., Milford, MA, USA). The separation of analytes was carried out using Acquity BEH C18 100 mm × 2.1 mm column (particle size, 1.7 μm) obtained from Waters, Ireland. The solvent system consisted of water with 0.1 % formic acid (A) and acetonitrile with 0.1 % formic acid (B). HPLC-method: flow rate was set at 200 μL/min. The percentage of B started at an initial of 5 %, held for 1 min, then gradually increased to 100 % over 10 min, maintained at 100 % for 2 min, and flushed back to 5 % over 3 min, then held at 5 % for 1 min. The MS scan was conducted under the following conditions: capillary voltage 3.5 kV, cone voltage 20 V, radio frequency (RF) lens voltage 2.5 V, source temperature set at 150 °C and desolvation gas temperature at 500 °C. Nitrogen served as the desolvation and cone gas at a flow rate of 1000 and 20 L/h, respectively. System operation and data acquisition were controlled using Mass Lynx 4.1 software (Waters). Melting points were measured using a Büchi B-540 melting point apparatus.

4.2. Procedure A: General procedure for the synthesis of intermediates A and B through Suzuki-Miyaura cross-coupling reaction

A stirred mixture of 5-bromo-1*H*-indazol-3-amine (2.5 mmol, 1 equiv), appropriate pyridine boronic acid (10 mmol, 4 equiv), Cs$_2$CO$_3$ (10 mmol, 4 equiv), and [Pd(dppf)Cl$_2$] (0.25 mmol, 0.1 equiv) dissolved in 60 mL 1,4-dioxane and 15 mL water in a ratio of 4 (1,4-dioxane): 1 (water) was refluxed overnight. Afterwards, the mixture was concentrated under vacuum and the residue was partitioned between ethyl acetate (50 mL) and brine solution (50 mL). This was followed by the re-extraction of the aqueous layer three times, each with an additional 50 mL of ethyl acetate. The organic layers were collected and dried over anhydrous MgSO$_4$ then the ethyl acetate was completely evaporated under reduced pressure. The resulting residue was then isolated using the recrystallization technique by completely dissolving the residue in 7 mL DCM (acting as the good solvent) and heating the flask at 60 °C with continuous stirring. Drops of DCM were added until the solution was almost clear then *n*-hexane (acting as the bad solvent) was added until persistent turbidity appeared. The flask was then allowed to cool to room temperature and then placed in an ice bath for 10 min and the precipitate was filtered, collected, and used in the next step.

4.2.1. 5-(Pyridin-3-yl)-1H-indazol-3-amine (A)

Intermediate **A** was prepared according to procedure A using pyridin-3-ylboronic acid to give a grayish-white solid: yield of 69 %; mp 200.2–202.2 °C; ^{1}H NMR (400 MHz, DMSO-d_6) δ 11.55 (s, 1H), 8.93 (s, 1H), 8.51 (d, *J* = 4.0 Hz, 1H), 8.11 (s, 1H), 8.04 (d, *J* = 7.8 Hz, 1H), 7.61 (d, *J* = 8.5 Hz, 1H), 7.47 (dd, *J* = 7.5, 4.8 Hz, 1H), 7.35 (d, *J* = 8.6 Hz, 1H), 5.48 (s, 2H); ^{13}C NMR (101 MHz, DMSO-d_6) δ 150.2, 147.8, 141.45, 137.0, 134.0, 126.9, 125.8, 124.3, 119.3, 115.3, 110.6; (ESI-MS) *m/z* = 211.09 [M + H]$^+$.

4.2.2. 5-(Pyridin-4-yl)-1H-indazol-3-amine (B)

Intermediate **B** was prepared according to procedure A using

pyridin-4-ylboronic acid giving a grey solid; yield of 75 %; mp 191.1–193.1 °C; ^{1}H NMR (400 MHz, DMSO-d_6) δ 11.61 (s, 1H), 8.59 (d, *J* = 4.0 Hz, 2H), 8.25 (s, 1H), 7.71 – 7.65 (m, 3H), 7.35 (d, *J* = 8.7 Hz, 1H), 5.54 (s, 2H); ^{13}C NMR (101 MHz, DMSO-d_6) δ 150.3, 150.2, 148.0, 141.7, 126.6, 125.2, 120.9, 119.5, 115.0, 110.4; (ESI-MS) *m/z* = 211.09 [M + H]$^+$.

4.3. Procedure B: General procedure for the synthesis of compounds 1–25 through amide coupling of intermediates A/B

A mixture of **A/B** (0.5 mmol, 1 equiv), appropriate acetic acid (1 mmol, 2 equiv), EDC (1 mmol, 2 equiv), and DMAP (1 mmol, 2 equiv) was dissolved in 50 mL DCM and stirred overnight at room temperature. Upon completion, DCM was removed under reduced pressure and the resulting residue was partitioned between ethyl acetate (50 mL) and water (30 mL). Re-extraction of the aqueous layer was done once using ethyl acetate (30 mL). The organic layers were combined, dried over anhydrous MgSO$_4$, and evaporated under vacuum. The product was then purified by CC.

4.3.1. 1-[3-Amino-5-(pyridin-3-yl)-1H-indazol-1-yl]-2-phenylethan-1-one (1)

Compound **1** was prepared according to procedure B using phenyl acetic acid to give a yellowish-white solid with yield of 36 %; The product was purified by CC (DCM/MeOH 100:5); mp 197.5–199.5 °C; ^{1}H NMR (500 MHz, DMSO-d_6) δ 8.93 (t, *J* = 3.9 Hz, 1H), 8.59 (dd, *J* = 4.7, 1.5 Hz, 1H), 8.32 (d, *J* = 1.2 Hz, 1H), 8.29 (d, *J* = 8.6 Hz, 1H), 8.11 (ddd, *J* = 8.0, 2.3, 1.7 Hz, 1H), 7.93 (dd, *J* = 8.6, 1.8 Hz, 1H), 7.55 – 7.51 (m, 1H), 7.37 – 7.32 (m, 3H), 7.26 (ddd, *J* = 8.6, 3.0, 1.5 Hz, 1H), 6.63 (s, 2H), 4.34 (s, 2H); ^{13}C NMR (126 MHz, DMSO-d_6) δ 169.4, 152.9, 148.5, 147.6, 138.9, 135.2, 135.0, 134.1, 132.7, 129.7, 128.7, 128.3, 126.6, 124.0, 121.1, 119.2, 115.7, 40.7; (ESI-MS) *m/z* = 329.13 [M + H]$^+$.

4.3.2. 1-[3-Amino-5-(pyridin-4-yl)-1H-indazol-1-yl]-2-(2-fluorophenyl)ethan-1-one (2)

Compound **2** was prepared according to procedure B using 2-fluoro-phenyl acetic acid to give a white solid: yield (38 %); The product was purified by CC (DCM/MeOH 100:5); mp 200.2–202.2 °C; ^{1}H NMR (500 MHz, DMSO-d_6) δ 8.69 (t, *J* = 11.4 Hz, 2H), 8.45 (s, 1H), 8.27 (d, *J* = 8.6 Hz, 1H), 8.03 (d, *J* = 8.4 Hz, 1H), 7.74 (d, *J* = 4.9 Hz, 2H), 7.44 (t, *J* = 7.2 Hz, 1H), 7.39 – 7.33 (m, 1H), 7.20 (dd, *J* = 17.6, 9.2 Hz, 2H), 6.70 (s, 2H), 4.42 (s, 2H); ^{13}C NMR (126 MHz, DMSO-d_6) δ 168.3, δ 160.9 (d, $^1J_{C\text{-}F}$ = 244.3 Hz), 153.1, 150.6, 150.4, 146.5, 139.5, 132.8, 132.4 (d, $^3J_{C\text{-}F}$ = 4.3 Hz), 129.1 (d, $^3J_{C\text{-}F}$ = 8.1 Hz), 128.6, 124.3 (d, $^4J_{C\text{-}F}$ = 3.2 Hz), 122.1 (d, $^2J_{C\text{-}F}$ = 16.0 Hz), 121.1, 119.5, 115.5, 115.0 (d, $^2J_{C\text{-}F}$ = 21.3 Hz), 34.64; (ESI-MS) *m/z* = 347.12 [M + H]$^+$.

4.3.3. 1-[3-Amino-5-(pyridin-4-yl)-1H-indazol-1-yl]-2-(3-fluorophenyl)ethan-1-one (3)

Compound **3** was prepared according to procedure B using 3-fluoro-phenyl acetic acid to give a white solid: yield (35 %); The product was purified by CC (DCM/MeOH 100:5); mp 205.5–207.5 °C; ^{1}H NMR (500 MHz, DMSO-d_6) δ 8.67 (d, *J* = 5.9 Hz, 2H), 8.44 (s, 1H), 8.29 (d, *J* = 8.6 Hz, 1H), 8.02 (dd, *J* = 8.7, 1.4 Hz, 1H), 7.73 (t, *J* = 8.8 Hz, 2H), 7.40 – 7.33 (m, 1H), 7.21 (t, *J* = 10.0 Hz, 2H), 7.10 (td, *J* = 8.9, 2.4 Hz, 1H), 6.68 (s, 2H), 4.38 (s, 2H); ^{13}C NMR (126 MHz, DMSO-d_6) δ 169.0, 162.0 (d, $^1J_{C\text{-}F}$ = 242.8 Hz), 153.0, 150.4, 146.5, 139.5, 137.7 (d, $^3J_{C\text{-}F}$ = 8.1 Hz), 132.8, 130.1 (d, $^3J_{C\text{-}F}$ = 8.4 Hz), 128.6, 126.0 (d, $^4J_{C\text{-}F}$ = 2.6 Hz), 121.2, 121.1, 119.5, 116.7 (d, $^2J_{C\text{-}F}$ = 21.3 Hz), 115.6, 113.5 (d, $^2J_{C\text{-}F}$ = 20.7 Hz), 40.4; (ESI-MS) *m/z* = 347.12 [M + H]$^+$.

4.3.4. 1-[3-Amino-5-(pyridin-4-yl)-1H-indazol-1-yl]-2-(4-fluorophenyl)ethan-1-one (4)

Compound **4** was prepared according to procedure B using 4-fluoro-phenyl acetic acid to give a white solid: yield (38 %); The product was

purified by CC (DCM/MeOH 100:5); mp 210.4–212.4 °C; ^{1}H NMR (500 MHz, DMSO-d_6) δ 8.67 (dd, J = 4.6, 1.5 Hz, 2H), 8.43 (d, J = 1.4 Hz, 1H), 8.28 (d, J = 8.6 Hz, 1H), 8.01 (dd, J = 8.7, 1.7 Hz, 1H), 7.73 (dd, J = 4.6, 1.6 Hz, 2H), 7.43 – 7.36 (m, 2H), 7.19 – 7.13 (m, 2H), 6.67 (s, 2H), 4.34 (s, 2H); ^{13}C NMR (126 MHz, DMSO-d_6) δ 169.5, 163.3, 161.2 (d, [1]$J_{C\text{-}F}$ = 242.2 Hz), 153.1, 150.4, 146.6, 139.6, 132.7, 131.7 (d, [3]$J_{C\text{-}F}$ = 8.0 Hz), 131.4 (s, [3]$J_{C\text{-}F}$ = 7.8 Hz), δ 131.2 (d, [4]$J_{C\text{-}F}$ = 2.8 Hz), 128.6, 121.2, 119.5, 115.6, 115.0 (d, [2]$J_{C\text{-}F}$ = 21.2 Hz), 115.0 (d, [2]$J_{C\text{-}F}$ = 21.2 Hz), 39.9; (ESI-MS) m/z = 347.12 [M + H]$^+$.

4.3.5. 1-[3-Amino-5-(pyridin-4-yl)-1H-indazol-1-yl]-2-(2-chlorophenyl)ethan-1-one (5)

Compound 5 was prepared according to procedure B using 2-chlorophenyl acetic acid to give a yellowish-white solid: yield (36 %); The product was purified by CC (DCM/MeOH 100:5); mp 202.7–204.7 °C; ^{1}H NMR (500 MHz, DMSO-d_6) δ 8.68 (dd, J = 4.7, 1.4 Hz, 2H), 8.45 (d, J = 1.2 Hz, 1H), 8.27 (d, J = 8.6 Hz, 1H), 8.03 (dd, J = 8.7, 1.7 Hz, 1H), 7.75 (dd, J = 4.6, 1.6 Hz, 2H), 7.52 – 7.46 (m, 2H), 7.37 – 7.32 (m, 2H), 6.70 (s, 2H), 4.52 (s, 2H); ^{13}C NMR (126 MHz, DMSO-d_6) δ 168.2, 153.1, 150.4, 146.6, 139.5, 133.9, 133.3, 132.8, 132.6, 129.0, 128.9, 128.6, 127.1, 121.2, 121.1, 119.5, 115.5; (ESI-MS) m/z = 363.09 [M + H]$^+$.

4.3.6. 1-[3-Amino-5-(pyridin-4-yl)-1H-indazol-1-yl]-2-(3-chlorophenyl)ethan-1-one (6)

Compound 6 was prepared according to procedure D using 3-chlorophenyl acetic acid to give a yellowish-white solid: yield (36 %); The product was purified by CC (DCM/MeOH 100:5); mp 199.3–201.3 °C; ^{1}H NMR (500 MHz, DMSO-d_6) δ 8.68 (dd, J = 4.6, 1.5 Hz, 2H), 8.44 (d, J = 1.2 Hz, 1H), 8.29 (d, J = 8.6 Hz, 1H), 8.04 – 8.01 (m, 1H), 7.74 (dd, J = 4.6, 1.6 Hz, 2H), 7.46 (s, 1H), 7.35 (dt, J = 11.0, 6.7 Hz, 3H), 6.69 (s, 2H), 4.38 (s, 2H); ^{13}C NMR (126 MHz, DMSO-d_6) δ 169.5, 153.5, 150.8, 147.0, 140.0, 137.9, 133.2, 133.2, 130.5, 130.2, 129.1, 129.0, 127.2, 121.6, 121.6, 119.9, 116.0, 40.8; (ESI-MS) m/z = 363.09 [M + H]$^+$.

4.3.7. 1-[3-Amino-5-(pyridin-4-yl)-1H-indazol-1-yl]-2-(4-chlorophenyl)ethan-1-one (7)

Compound 7 was prepared according to procedure B using 4-chlorophenyl acetic acid to give a yellowish-white solid: yield (35 %); The product was purified by CC (DCM/MeOH 100:5); mp 209.5–211.5 °C; ^{1}H NMR (500 MHz, DMSO-d_6) δ 8.67 (d, J = 6.0 Hz, 2H), 8.43 (d, J = 1.0 Hz, 1H), 8.28 (d, J = 8.6 Hz, 1H), 8.00 (dd, J = 8.7, 1.6 Hz, 1H), 7.72 (d, J = 6.1 Hz, 2H), 7.38 (s, 4H), 6.67 (s, 2H), 4.35 (s, 2H); ^{13}C NMR (126 MHz, DMSO-d_6) δ 169.1, 153.0, 150.4, 146.5, 139.5, 134.0, 132.7, 131.7, 131.4, 128.5, 128.2, 121.2, 121.1, 119.4, 115.6, 40.1; (ESI-MS) m/z = 363.09 [M + H]$^+$.

4.3.8. 1-[3-Amino-5-(pyridin-4-yl)-1H-indazol-1-yl]-2-(2-bromophenyl)ethan-1-one (8)

Compound 8 was prepared according to procedure B using 2-bromophenyl acetic acid to give a yellowish-white solid: yield (30 %); The product was purified by CC (DCM/MeOH 100:5); mp 205.8–207.8 °C; ^{1}H NMR (500 MHz, DMSO-d_6) δ 8.68 (d, J = 6.0 Hz, 2H), 8.45 (d, J = 1.3 Hz, 1H), 8.27 (d, J = 8.6 Hz, 1H), 8.03 (dd, J = 8.7, 1.7 Hz, 1H), 7.75 (dd, J = 4.6, 1.5 Hz, 2H), 7.66 – 7.61 (m, 1H), 7.49 (dd, J = 7.6, 1.5 Hz, 1H), 7.39 (td, J = 7.5, 0.9 Hz, 1H), 7.26 (td, J = 7.8, 1.6 Hz, 1H), 6.71 (s, 2H), 4.53 (s, 2H); ^{13}C NMR (126 MHz, DMSO-d_6) δ 168.2, 153.1, 150.4, 146.6, 139.5, 135.1, 132.8, 132.7, 132.2, 129.1, 128.6, 127.7, 124.8, 121.2, 121.1, 119.5, 115.5, 41.7; (ESI-MS) m/z = 407.04 [M + H]$^+$.

4.3.9. 1-[3-Amino-5-(pyridin-4-yl)-1H-indazol-1-yl]-2-(3-bromophenyl)ethan-1-one (9)

Compound 9 was prepared according to procedure B using 3-bromophenyl acetic acid to give a yellowish-white solid: yield (32 %); The product was purified by CC (DCM/MeOH 100:5); mp 211.9–213.9 °C; ^{1}H NMR (500 MHz, DMSO-d_6) δ 8.67 (dd, J = 4.6, 1.6 Hz, 2H), 8.43 (d, J = 1.2 Hz, 1H), 8.28 (d, J = 8.6 Hz, 1H), 8.02 (dd, J = 8.7, 1.8 Hz, 1H), 7.73 (dd, J = 4.6, 1.6 Hz, 2H), 7.58 (d, J = 1.6 Hz, 1H), 7.48 – 7.45 (m, 1H), 7.36 (d, J = 7.7 Hz, 1H), 7.30 (t, J = 7.8 Hz, 1H), 6.68 (s, 2H), 4.37 (s, 2H); ^{13}C NMR (126 MHz, DMSO-d_6) δ 169.0, 153.1, 150.4, 146.5, 139.5, 137.7, 132.8, 132.6, 130.4, 129.6, 129.1, 128.6, 128.6, 121.4, 121.1, 119.5, 115.6, 40.3; (ESI-MS) m/z = 407.04 [M + H]$^+$.

4.3.10. 1-[3-Amino-5-(pyridin-4-yl)-1H-indazol-1-yl]-2-(4-bromophenyl)ethan-1-one (10)

Compound 10 was prepared according to procedure B using 4-bromophenyl acetic acid to give a yellowish-white solid: yield (30 %); The product was purified by CC (DCM/MeOH 100:5); mp 198.8–200.8 °C; ^{1}H NMR (500 MHz, DMSO-d_6) δ 8.68 (dd, J = 4.7, 1.4 Hz, 2H), 8.44 (d, J = 1.4 Hz, 1H), 8.29 (d, J = 8.6 Hz, 1H), 8.02 (dd, J = 8.7, 1.7 Hz, 1H), 7.75 – 7.72 (m, 2H), 7.53 (d, J = 8.3 Hz, 2H), 7.33 (d, J = 8.3 Hz, 2H), 6.67 (s, 2H), 4.34 (s, 2H); ^{13}C NMR (126 MHz, DMSO-d_6) δ 169.1, 153.0, 150.4, 146.5, 139.5, 134.5, 132.8, 132.1, 131.1, 128.6, 121.2, 121.1, 119.9, 119.5, 115.6, 40.2; (ESI-MS) m/z = 407.04 [M + H]$^+$.

4.3.11. 1-[3-Amino-5-(pridin-4-yl)-1H-indazol-1-yl]-2-[2-(trifluoromethyl)phenyl]ethan-1-one (11)

Compound 11 was prepared according to procedure B using 2-(trifluoromethyl)phenyl acetic acid to give a white solid: yield (36 %); The product was purified by CC (DCM/MeOH 100:5); mp 210.0–212.0 °C; ^{1}H NMR (500 MHz, DMSO-d_6) δ 8.68 (d, J = 4.0 Hz, 2H), 8.46 (s, 1H), 8.24 (d, J = 8.5 Hz, 1H), 8.01 (d, J = 8.4 Hz, 1H), 7.75 (d, J = 6.9 Hz, 3H), 7.68 (t, J = 7.2 Hz, 1H), 7.60 (d, J = 7.3 Hz, 1H), 7.53 (t, J = 7.3 Hz, 1H), 6.73 (s, 2H), 4.61 (s, 2H); ^{13}C NMR (126 MHz, DMSO-d_6) δ 168.5, 153.1, 150.4, 146.5, 139.5, 133.9, 133.2, 132.8, 132.3, 128.6, 127.8 (q, [2]$J_{C\text{-}F}$ = 29.4 Hz), 127.6, 125.7 (q, [3]$J_{C\text{-}F}$ = 5.4 Hz), 124.5 (q, [1]$J_{C\text{-}F}$ = 273.9 Hz), 121.1, 121.1, 119.5, 115.4, 38.3; (ESI-MS) m/z = 397.12 [M + H]$^+$.

4.3.12. 1-[3-Amino-5-(pyridin-4-yl)-1H-indazol-1-yl]-2-[3-(trifluoromethyl)phenyl]ethan-1-one (12)

Compound 12 was prepared according to procedure B using 3-(trifluoromethyl)phenyl acetic acid to give a white solid: yield (39 %); The product was purified by CC (DCM/MeOH 100:5); mp 199.3–201.3 °C; ^{1}H NMR (500 MHz, DMSO-d_6) δ 8.68 (d, J = 6.1 Hz, 2H), 8.45 (d, J = 1.1 Hz, 1H), 8.29 (d, J = 8.6 Hz, 1H), 8.02 (dd, J = 8.7, 1.6 Hz, 1H), 7.76 (s, 1H), 7.75 – 7.73 (m, 2H), 7.68 (d, J = 7.6 Hz, 1H), 7.64 (d, J = 7.8 Hz, 1H), 7.58 (t, J = 7.7 Hz, 1H), 6.70 (s, 2H), 4.50 (s, 2H); ^{13}C NMR (126 MHz, DMSO-d_6) δ 169.0, 153.1, 150.4, 146.5, 139.5, 136.4, 134.2, 132.7, 129.2, 128.9 (q, [2]$J_{C\text{-}F}$ = 31.3 Hz), 128.6, 126.6 (q, [4]$J_{C\text{-}F}$ = 3.7 Hz), 124.3 (q, [1]$J_{C\text{-}F}$ = 272.3 Hz), 123.5 (q, [4]$J_{C\text{-}F}$ = 3.5 Hz), 121.2, 121.1, 119.5, 115.6, 40.4; (ESI-MS) m/z = 397.12 [M + H]$^+$.

4.3.13. 1-[3-Amino-5-(pridin-4-yl)-1H-indazol-1-yl]-2-[4-(trifluoromethyl)phenyl]ethan-1-one (13)

Compound 13 was prepared according to procedure B using 4-(trifluoromethyl)phenyl acetic acid to give a white solid: yield (37 %); The product was purified by CC (DCM/MeOH 100:5); mp 208.4–210.4 °C; ^{1}H NMR (500 MHz, DMSO-d_6) δ 8.63 (d, J = 5.8 Hz, 2H), 8.40 (s, 1H), 8.25 (d, J = 8.6 Hz, 1H), 8.00 – 7.96 (m, 1H), 7.70 (d, J = 5.9 Hz, 2H), 7.67 (d, J = 8.1 Hz, 2H), 7.55 (d, J = 8.0 Hz, 2H), 6.65 (s, 2H), 4.43 (s, 2H); ^{13}C NMR (126 MHz, DMSO-d_6) δ 168.9, 153.2, 153.1, 150.4, 146.6, 139.9, 139.6, 132.8, 130.8, 128.6, 127.5 (q, [2]$J_{C\text{-}F}$ = 31.8 Hz), 125.1 (q, [4]$J_{C\text{-}F}$ = 3.7 Hz), 121.2, 121.2, 119.5, 115.6, 40.6; (ESI-MS) m/z = 397.12 [M + H]$^+$.

4.3.14. 1-[3-Amino-5-(pyridin-4-yl)-1H-indazol-1-yl]-2-(2-nitrophenyl)ethan-1-one (14)

Compound 14 was prepared according to procedure B using 2-nitrophenyl acetic acid to give a yellowish-white solid: yield (30 %); The product was purified by CC (DCM/MeOH 100:5); mp 211.2–213.2 °C; ^{1}H NMR (500 MHz, DMSO-d_6) δ 8.68 (d, J = 4.6 Hz, 2H), 8.46 (d, J = 4.6 Hz, 1H), 8.22 – 8.19 (m, 1H), 8.17 – 8.14 (m, 1H), 8.01 (dd, J = 7.6,

6.0 Hz, 1H), 7.81 – 7.74 (m, 3H), 7.69 – 7.66 (m, 1H), 7.62 (d, *J* = 6.7 Hz, 1H), 6.71 (s, 2H), 4.79 (d, *J* = 5.3 Hz, 2H); ^{13}C NMR (126 MHz, DMSO-d_6) δ 168.1, 153.1, 150.4, 148.8, 146.5, 139.4, 134.2, 133.9, 132.8, 130.4, 128.8, 128.6, 124.8, 121.2, 121.1, 119.5, 115.4, 39.9; (ESI-MS) *m/z* = 374.37 [M + H]$^+$.

4.3.15. 1-[3-Amino-5-(pyridin-4-yl)-1H-indazol-1-yl]-2-(3-nitrophenyl) ethan-1-one (15)

Compound **15** was prepared according to procedure B using 3-nitrophenyl acetic acid to give a yellowish-white solid: yield (32 %); The product was purified by CC (DCM/MeOH 100:5); mp 198.5–200.5 °C; ^{1}H NMR (500 MHz, DMSO-d_6) δ 8.68 (dd, *J* = 4.6, 1.6 Hz, 2H), 8.46 (d, *J* = 1.2 Hz, 1H), 8.31 – 8.28 (m, 2H), 8.19 – 8.13 (m, 1H), 8.03 (dd, *J* = 8.7, 1.8 Hz, 1H), 7.84 (d, *J* = 7.7 Hz, 1H), 7.75 (dd, *J* = 4.6, 1.6 Hz, 2H), 7.66 (t, *J* = 7.9 Hz, 1H), 6.71 (s, 2H), 4.56 (s, 2H); ^{13}C NMR (126 MHz, DMSO-d_6) δ 168.8, 153.1, 150.4, 147.7, 146.5, 139.5, 137.3, 137.0, 132.8, 129.6, 128.6, 124.8, 121.8, 121.2, 121.1, 119.5, 115.6, 40.2; (ESI-MS) *m/z* = 374.37 [M + H]$^+$.

4.3.16. 1-[3-Amino-5-(pyridin-4-yl)-1H-indazol-1-yl]-2-(o-tolyl)ethan-1-one (16)

Compound **16** was prepared according to procedure B using 2-methylphenyl acetic acid to give a yellowish-white solid: yield (34 %); The product was purified by CC (DCM/MeOH 100:5); mp 206.4–208.4 °C; ^{1}H NMR (500 MHz, DMSO-d_6) δ 8.68 (dd, *J* = 4.7, 1.4 Hz, 2H), 8.45 (d, *J* = 1.3 Hz, 1H), 8.29 (d, *J* = 8.6 Hz, 1H), 8.02 (dd, *J* = 8.7, 1.7 Hz, 1H), 7.74 (dd, *J* = 4.6, 1.5 Hz, 2H), 7.27 (d, *J* = 7.0 Hz, 1H), 7.21 – 7.12 (m, 3H), 6.67 (s, 2H), 4.37 (s, 2H), 2.27 (s, 3H); ^{13}C NMR (126 MHz, DMSO-d_6) δ 169.3, 153.0, 150.4, 146.6, 139.5, 136.9, 133.8, 132.7, 130.4, 129.9, 128.5, 126.9, 125.8, 121.1, 121.1, 119.4, 115.6, 38.7, 19.3; (ESI-MS) *m/z* = 343.15 [M + H]$^+$.

4.3.17. 1-[3-Amino-5-(pyridin-4-yl)-1H-indazol-1-yl]-2-(p-tolyl)ethan-1-one (17)

Compound **17** was prepared according to procedure B using 4-methylphenyl acetic acid to give a yellowish-white solid: yield (31 %); The product was purified by CC (DCM/MeOH 100:5); mp 197.9–199.9 °C; ^{1}H NMR (500 MHz, DMSO-d_6) δ 8.67 (dd, *J* = 4.7, 1.4 Hz, 2H), 8.43 (d, *J* = 1.3 Hz, 1H), 8.29 (d, *J* = 8.6 Hz, 1H), 8.00 (dd, *J* = 8.7, 1.7 Hz, 1H), 7.73 (dd, *J* = 4.7, 1.5 Hz, 2H), 7.24 (d, *J* = 7.9 Hz, 2H), 7.13 (d, *J* = 7.7 Hz, 2H), 6.65 (s, 2H), 4.28 (s, 2H), 2.27 (d, *J* = 4.2 Hz, 3H); ^{13}C NMR (126 MHz, DMSO-d_6) δ 169.5, 152.8, 150.2, 146.4, 139.4, 135.5, 132.5, 131.7, 129.4, 129.0, 128.7, 128.6, 121.0, 119.2, 115.4, 40.2, 20.5; (ESI-MS) *m/z* = 343.15 [M + H]$^+$.

4.3.18. 1-[3-Amino-5-(pyridin-4-yl)-1H-indazol-1-yl]-2-(2-methoxyphenyl)ethan-1-one (18)

Compound **18** was prepared according to procedure B using 2-methoxyphenyl acetic acid to give a yellowish-white solid: yield (32 %); The product was purified by CC (DCM/MeOH 100:5); mp 212.5–214.5 °C; ^{1}H NMR (500 MHz, DMSO-d_6) δ 8.68 (d, *J* = 5.8 Hz, 2H), 8.44 (s, 1H), 8.27 (d, *J* = 8.6 Hz, 1H), 8.01 (dd, *J* = 8.7, 1.4 Hz, 1H), 7.74 (d, *J* = 6.0 Hz, 2H), 7.30 – 7.22 (m, 2H), 7.00 (d, *J* = 8.2 Hz, 1H), 6.92 (t, *J* = 7.4 Hz, 1H), 6.64 (s, 2H), 4.30 (s, 2H), 3.74 (d, *J* = 9.2 Hz, 3H); ^{13}C NMR (126 MHz, DMSO-d_6) δ 169.4, 157.4, 152.8, 150.4, 146.6, 139.5, 132.5, 131.3, 128.5, 128.3, 123.4, 121.1, 120.9, 120.1, 119.4, 115.5, 110.7, 55.4, 35.8; (ESI-MS) *m/z* = 359.14 [M + H]$^+$.

4.3.19. 1-[3-Amino-5-(pyridin-4-yl)-1H-indazol-1-yl]-2-(3-methoxyphenyl)ethan-1-one (19)

Compound **19** was prepared according to procedure B using 3-methoxyphenyl acetic acid to give a yellowish-white solid: yield (33 %); The product was purified by CC (DCM/MeOH 100:5); mp 202.9–204.9 °C; ^{1}H NMR (500 MHz, DMSO-d_6) δ 8.68 (dd, *J* = 4.6, 1.5 Hz, 2H), 8.44 (d, *J* = 1.3 Hz, 1H), 8.30 (d, *J* = 8.6 Hz, 1H), 8.02 (dd, *J* = 8.7, 1.7 Hz, 1H), 7.74 (dd, *J* = 4.6, 1.5 Hz, 2H), 7.24 (t, *J* = 7.9 Hz, 1H), 6.94 (dd, *J* = 13.1, 4.8 Hz, 2H), 6.85 – 6.81 (m, 1H), 6.66 (s, 2H), 4.31 (s, 2H), 3.74 (s, 3H); ^{13}C NMR (126 MHz, DMSO-d_6) δ 169.4, 159.2, 153.0, 150.4, 146.5, 139.5, 136.4, 132.7, 129.3, 128.5, 121.9, 121.2, 121.1, 119.4, 115.6, 115.6, 112.0, 55.0, 40.8; (ESI-MS) *m/z* = 359.14 [M + H]$^+$.

4.3.20. 1-[3-Amino-5-(pyridin-4-yl)-1H-indazol-1-yl]-2-(4-methoxyphenyl)ethan-1-one (20)

Compound **20** was prepared according to procedure B using 4-methoxyphenyl acetic acid to give a yellowish-white solid: yield (31 %); The product was purified by CC (DCM/MeOH 100:5); mp 197.6–199.6 °C; ^{1}H NMR (500 MHz, DMSO-d_6) δ 8.67 (dd, *J* = 4.6, 1.5 Hz, 2H), 8.43 (d, *J* = 1.3 Hz, 1H), 8.29 (d, *J* = 8.6 Hz, 1H), 8.01 (dd, *J* = 8.4, 1.4 Hz, 1H), 7.73 (dd, *J* = 4.6, 1.5 Hz, 2H), 7.27 (d, *J* = 8.6 Hz, 2H), 6.88 (t, *J* = 5.8 Hz, 2H), 6.64 (s, 2H), 4.26 (s, 2H), 3.73 (s, 3H); ^{13}C NMR (126 MHz, DMSO-d_6) δ 169.8, 158.1, 152.9, 150.4, 150.4, 146.5, 139.6, 132.6, 130.7, 128.5, 126.8, 121.1, 119.4, 115.6, 113.7, 55.1; (ESI-MS) *m/z* = 359.14 [M + H]$^+$.

4.3.21. 1-[3-Amino-5-(pyridin-4-yl)-1H-indazol-1-yl]-2-(3-hydroxyphenyl)ethan-1-one (21)

Compound **21** was prepared according to procedure B using 3-hydroxyphenyl acetic acid to give a yellowish-white solid: yield (39 %); The product was purified by CC (DCM/MeOH 100:6); mp 208.5–210.5 °C; ^{1}H NMR (400 MHz, DMSO-d_6) δ 9.33 (s, 1H), 8.67 (d, *J* = 5.7 Hz, 2H), 8.43 (s, 1H), 8.31 (d, *J* = 8.6 Hz, 1H), 8.02 (d, *J* = 8.5 Hz, 1H), 7.74 (d, *J* = 5.8 Hz, 2H), 7.10 (t, *J* = 7.9 Hz, 1H), 6.76 (d, *J* = 7.1 Hz, 2H), 6.64 (s, 3H), 4.24 (s, 2H); ^{13}C NMR (101 MHz, DMSO-d_6) δ 169.5, 157.3, 152.9, 150.3, 146.5, 139.5, 136.2, 132.7, 129.2, 128.5, 121.2, 121.1, 120.2, 119.4, 116.4, 115.6, 113.6, 40.6; (ESI-MS) *m/z* = 345.13 [M + H]$^+$.

4.3.22. 1-[3-Amino-5-(pyridin-4-yl)-1H-indazol-1-yl]-2-(4-hydroxyphenyl)ethan-1-one (22)

Compound **22** was prepared according to procedure B using 4-hydroxyphenyl acetic acid to give a yellowish-white solid: yield (32 %); The product was purified by CC (DCM/MeOH 100:6); mp 206.7–208.7 °C; ^{1}H NMR (500 MHz, DMSO-d_6) δ 9.30 (s, 1H), 8.70 – 8.66 (m, 2H), 8.43 (d, *J* = 1.2 Hz, 1H), 8.30 (d, *J* = 8.6 Hz, 1H), 8.01 (dd, *J* = 8.7, 1.7 Hz, 1H), 7.74 (dd, *J* = 4.6, 1.6 Hz, 2H), 7.15 (d, *J* = 8.5 Hz, 2H), 6.73 – 6.69 (m, 2H), 6.64 (s, 2H), 4.20 (s, 2H); ^{13}C NMR (126 MHz, DMSO-d_6) δ 170.0, 156.2, 152.9, 150.4, 146.6, 139.6, 132.6, 130.7, 128.5, 125.0, 121.1, 119.4, 118.1, 115.6, 115.1; (ESI-MS) *m/z* = 345.13 [M + H]$^+$.

4.3.23. 1-[3-Amino-5-(pyridin-4-yl)-1H-indazol-1-yl]-2-(naphthalen-2-yl)ethan-1-one (23)

Compound **23** was prepared according to procedure B using 2-napthylacetic acid to give a white solid: yield (35 %); The product was purified by CC (DCM/MeOH 100:5); mp 209.9–211.9 °C; ^{1}H NMR (500 MHz, DMSO-d_6) δ 8.67 (d, *J* = 5.6 Hz, 2H), 8.45 (s, 1H), 8.31 (d, *J* = 8.6 Hz, 1H), 8.01 (d, *J* = 8.6 Hz, 1H), 7.88 (d, *J* = 9.3 Hz, 4H), 7.74 (d, *J* = 5.8 Hz, 2H), 7.56 – 7.52 (m, 1H), 7.49 (dd, *J* = 9.1, 5.7 Hz, 2H), 6.69 (s, 2H), 4.52 (s, 2H); ^{13}C NMR (126 MHz, DMSO-d_6) δ 169.5, 153.0, 150.4, 146.5, 139.6, 133.0, 132.7, 132.7, 131.9, 128.5, 128.3, 128.1, 127.7, 127.5, 127.4, 126.1, 125.7, 121.2, 121.1, 119.4, 115.6, 40.9; (ESI-MS) *m/z* = 379.15 [M + H]$^+$.

4.3.24. 1-[3-Amino-5-(pyridin-4-yl)-1H-indazol-1-yl]-2,2-diphenylethan-1-one (24)

Compound **24** was prepared according to procedure B using 2,2-diphenylacetic acid to give a yellowish-white solid: yield (36 %); The product was purified by CC (DCM/MeOH 100:5); mp 180.1–182.1 °C; ^{1}H NMR (500 MHz, DMSO-d_6) δ 8.67 (d, *J* = 5.4 Hz, 2H), 8.43 (s, 1H), 8.39 (d, *J* = 8.7 Hz, 1H), 8.04 (dd, *J* = 8.7, 1.4 Hz, 1H), 7.73 (d, *J* = 5.9 Hz, 2H), 7.36 – 7.34 (m, 6H), 7.26 (td, *J* = 5.8, 2.8 Hz, 2H), 6.67 (s, 2H),

6.42 (s, 1H), 5.75 (s, 2H); ^{13}C NMR (126 MHz, DMSO-d_6) 169.9, 153.1, 150.4, 146.5, 139.6, 139.3, 133.1, 128.8, 128.7, 128.5, 127.0, 121.5, 121.2, 119.5, 115.9, 54.0; (ESI-MS) m/z = 405.16 [M + H]$^+$.

4.3.25. 1-[3-Amino-5-(yridine-4-yl)-1H-indazol-1-yl]-2-phenoxyethan-1-one (25)

Compound **25** was prepared according to procedure B using phenoxyacetic acid to give a white solid: yield (32 %); The product was purified by CC (DCM/MeOH 100:5); mp 220.2–222.2 °C; ^{1}H NMR (400 MHz, DMSO-d_6) δ 8.68 (dd, J = 4.6, 1.6 Hz, 2H), 8.46 (d, J = 1.1 Hz, 1H), 8.26 (d, J = 8.6 Hz, 1H), 8.04 (dd, J = 8.6, 1.7 Hz, 1H), 7.74 (dd, J = 4.6, 1.6 Hz, 2H), 7.37 – 7.23 (m, 2H), 6.96 (t, J = 8.2 Hz, 3H), 6.75 (s, 2H), 5.42 (s, 2H); ^{13}C NMR (101 MHz, DMSO-d_6) 166.4, 158.4, 153.9, 150.8, 146.9, 139.8, 133.4, 129.9, 129.2, 121.6, 121.4, 121.3, 120.0, 115.6, 114.9, 66.0; (ESI-MS) m/z = 345.13 [M + H]$^+$.

4.4. Biological assays

4.4.1. Haspin kinase assay

The kinase assay was done at (Thermo Fisher Scientific, Madison, WI, USA) through a fluorescence-based immunoassay known as (The Adapta Universal Kinase Assay), which detects the ADP produced by kinases utilizing the TR-FRET technology. The final 10 μL kinase reaction consists of 0.25–1 ng GSG2 (haspin) and 100 μM of the substrate (Histone H3 (1–20) peptide) in 32.5 mM HEPES pH 7.5, 0.005 % BRIJ-35, 5 mM MgCl$_2$, 0.5 mM EGTA, in the presence of 25 μM ATP. After an incubation time of 1 hr at RT, 5 μL of a detection mix was added. Staurosporine (IC$_{50}$ = 7.7 nM) was used as a positive control. To determine the half-maximal inhibitory concentration (IC$_{50}$), the assays were performed in duplicates or triplicates with varying doses of the tested compounds. The GSG2 (Haspin) used is a GST tag recombinant protein derived from human tissue while using insect cells' expression system. The amino acid sequence used in this assay was from 471 to 798.

4.4.2. Clk4 kinase assay

The kinase assay was done at (Thermo Fisher Scientific, Madison, WI, USA) through a fluorescence-based immunoassay known as (The LanthaScreen Eu Kinase Binding Assay). This was done by binding an Alexa FluorTM conjugate or "tracer" to the kinase and this binding was detected by the addition of a Eu-labeled anti-tag antibody. The binding of the tracer and antibody to the kinase results in a high degree of FRET. On the other hand, displacement of the tracer with a kinase inhibitor results in a loss of FRET. The kinase concentration used is 5 nM added to it 2 nM of Eu-anti-GST antibody, 30 nM of tracer 236 with K$_d$ 28 nM, and buffer A (50 mM HEPES pH 7.5, 0.01 % BRIJ-35, 10 mM MgCl$_2$, 1 mM EGTA). Staurosporine (IC$_{50}$ = 7.02 nM) was used as a positive control. To determine the half-maximal inhibitory concentration (IC$_{50}$), the assays were performed in duplicates or triplicates with varying doses of the tested compounds. The Clk4 used is a GST-tagged, recombinant human protein, expressed in insect cells as a full length protein (ThermoFisher, Cat. No. PV3986).

4.4.3. Kinase selectivity profiling assays

For Dyrk2 and STK17A (DRAK1): the assay was done at (Thermo Fisher Scientific, Madison, WI, USA) through a fluorescence-based immunoassay known as (The LanthaScreen Eu Kinase Binding Assay).

For CDK5/p25, Clk 1–3, CSNK1D (CK1 delta), CSNK2A1 (CK2 alpha 1), Dyrk1A, Dyrk1B, HIPK1 (Myak), NTRK2 (TRKB), PIM1, and SRPK1: The kinase assay was done at (Thermo Fisher Scientific, Madison, WI, USA) through a fluorescence-based immunoassay known as (the Ź-LYTE biochemical assay).

4.4.4. Single-dose profiling against NCI-60 cancerous cell lines

Compounds **2**, **5**, **8**, **21**, and **22** were screened for their *in vitro* antiproliferative activity against 60 different cancerous cell lines representing nine different human tissues: leukemia, non-small cell lung cancer, melanoma, colon cancer, CNS cancer, breast cancer, ovarian cancer, renal cancer, prostate cancer at a single dose of 10 μM. This was done at the Developmental Therapeutics Program (DTP) of the National Cancer Institute (NCI) using the sulforhodamine B (SRB) assay[49]. The results represent growth percentages compared to the no-drug control and to the number of cells at time zero. From the values of mean growth percentages, percentages of growth inhibition (% GI) were computed as (100 - growth %).

4.5. In silico examinations

4.5.1. Calculated physicochemical and pharmacokinetic properties

The most potent haspin inhibitors compounds **5** and **21** were screened for their ADME parameters using online website "SwissADME". Moreover, the Swiss-ADME tool was used to predict the permeability of those 2 most potent compounds through the human gastrointestinal tract and blood–brain barrier.

4.5.2. Molecular docking

Docking studies were carried out essentially as described in ref.[55] and all procedures were performed using the Molecular Operating Environment (MOE) software package (version 2019. Chemical Computing Group). For the docking simulations, PDB entry: 7OPS (haspin co-crystallized with compound 2a: 2-(methylthio)-10-nitro-pyrido[3,4-g]quinazoline) was used. Molecular docking simulations with compound **21** as a ligand were performed using the MMFF94x force field and the "alpha pmi" method (number of return poses set to 100) and "Induced fit" as refinement. A pharmacophore was defined based on a suitable pose after energy minimization, by selecting both the *N* of pyridinyl as acceptor point and the amino group as acceptor or donor point. In the pharmacophore definition window, the radius of the pharmacophore points was raised to 1.6 Å. The subsequent docking of **21** in haspin's binding pocket was performed using the pharmacophore–supported placement. The number of retained poses was set to 100 each time. Only the poses with the top 10 scoring values were further evaluated for plausibility.

CRediT authorship contribution statement

Mona M. Shawky: Writing – review & editing, Writing – original draft, Data curation, Investigation, Methodology, Formal analysis. **Mennatallah Abdallah:** Writing – review & editing, Methodology, Investigation. **Hend Khalifa:** Writing – review & editing, Methodology, Investigation. **Youssef Aboushady:** Methodology, Investigation. **Ashraf H. Abadi:** Writing – review & editing, Supervision. **Matthias Engel:** Writing – review & editing, Writing – original draft, Supervision, Investigation, Funding acquisition, Conceptualization, Formal analysis, Methodology, Project administration. **Mohammad Abdel-Halim:** Writing – review & editing, Writing – original draft, Supervision, Project administration, Funding acquisition, Formal analysis, Conceptualization, Investigation, Methodology.

Declaration of competing interest

The authors declare that they have no known competing financial interests or personal relationships that could have appeared to influence the work reported in this paper.

Appendix A. Supplementary data

Supplementary data to this article can be found online at https://doi.org/10.1016/j.bioorg.2024.107235.

References

[1] V. Modi, R.L. Dunbrack, Defining a new nomenclature for the structures of active and inactive kinases, Proc. Natl. Acad. Sci. USA 116 (2019) 6818–6827, https://doi.org/10.1073/pnas.1814279116.

[2] P. Theivendren, S. Kunjiappan, Y. Mariappa Hegde, S. Vellaichamy, M. Gopal, S. Rajan Dhramalingam, S. Kumar, Importance of Protein Kinase and Its Inhibitor: A Review, in: Intech Open, 2021: pp. 225–240. https://doi.org/10.5772/intechopen.98552.

[3] D. Huertas, M. Soler, J. Moreto, A. Villanueva, A. Martinez, A. Vidal, M. Charlton, D. Moffat, S. Patel, J. McDermott, J. Owen, D. Brotherton, D. Krige, S. Cuthill, M. Esteller, Antitumor activity of a small-molecule inhibitor of the histone kinase Haspin, Oncogene 31 (2012) 1408–1418, https://doi.org/10.1038/onc.2011.335.

[4] C. Opoku-Temeng, N. Dayal, M. Aflaki Sooreshjani, H.O. Sintim, 3H-pyrazolo[4,3-f]quinoline haspin kinase inhibitors and anticancer properties, Bioorg. Chem. 78 (2018) 418–426, https://doi.org/10.1016/j.bioorg.2018.03.031.

[5] J. Eswaran, D. Patnaik, P. Filippakopoulos, F. Wang, R.L. Stein, J.W. Murray, J.M. G. Higgins, S. Knapp, Structure and functional characterization of the atypical human kinase haspin, Proc. Natl. Acad. Sci. USA 106 (2009) 20198–20203, https://doi.org/10.1073/pnas.0901989106.

[6] O. Feizbakhsh, M. Place, X. Fant, F. Buron, S. Routier, S. Ruchaud, The Mitotic Protein Kinase Haspin and Its Inhibitors, in: Protein Phosphorylation, InTech, 2017: p. 13. https://doi.org/10.5772/intechopen.70732.

[7] Y. Yoshimura, H. Tanaka, M. Nozaki, K. Yomogida, T. Yasunaga, Y. Nishimune, Nested genomic structure of haploid germ cell specific haspin gene, Gene 267 (2001) 49–54, https://doi.org/10.1016/S0378-1119(01)00386-9.

[8] K. Soupsana, E. Karanika, F. Kiosse, A. Christogianni, Y. Sfikas, P. Topalis, A. Batistatou, Z. Kanaki, A. Klinakis, A.S. Politou, S. Georgatos, Distinct roles of haspin in stem cell division and male gametogenesis, Sci. Rep. 11 (2021) 19901, https://doi.org/10.1038/s41598-021-99307-8.

[9] J.M.G. Higgins, Structure, function and evolution of haspin and haspin-related proteins, a distinctive group of eukaryotic protein kinases, Cell. Mol. Life Sci. 60 (2003) 446–462, https://doi.org/10.1007/s000180300038.

[10] N.G. Amoussou, A. Bigot, C. Roussakis, J.M.H. Robert, Haspin: a promising target for the design of inhibitors as potent anticancer drugs, Drug Discov. Today 23 (2018) 409–415, https://doi.org/10.1016/j.drudis.2017.10.005.

[11] J.M.G. Higgins, Haspin: a newly discovered regulator of mitotic chromosome behavior, Chromosoma 119 (2010) 137–147, https://doi.org/10.1007/s00412-009-0250-4.

[12] K. Kestav, A. Uri, D. Lavogina, Structure, Roles and Inhibitors of a Mitotic Protein Kinase Haspin, Curr. Med. Chem. 24 (2017) 2276–2293, https://doi.org/10.2174/0929867324666170414155520.

[13] G.D. Cuny, M. Robin, N.P. Ulyanova, D. Patnaik, V. Pique, G. Casano, J.-F. Liu, X. Lin, J. Xian, M.A. Glicksman, R.L. Stein, J.M.G. Higgins, Structure–activity relationship study of acridine analogs as haspin and DYRK2 kinase inhibitors, Bioorg. Med. Chem. Lett. 20 (2010) 3491–3494, https://doi.org/10.1016/j.bmcl.2010.04.150.

[14] A.E. Kelly, C. Ghenoiu, J.Z. Xue, C. Zierhut, H. Kimura, H. Funabiki, Survivin Reads Phosphorylated Histone H3 Threonine 3 to Activate the Mitotic Kinase Aurora B, Science (80-.). 330 (2010) 235–239. https://doi.org/10.1126/science.1189505.

[15] F. Wang, J. Dai, J.R. Daum, E. Niedzialkowska, B. Banerjee, P.T. Stukenberg, G.J. Gorbsky, J.M.G. Higgins, Histone H3 Thr-3 Phosphorylation by Haspin Positions Aurora B at Centromeres in Mitosis, Science (80-.). 330 (2010) 231–235. https://doi.org/10.1126/science.1189435.

[16] Y. Yamagishi, T. Honda, Y. Tanno, Y. Watanabe, Two Histone Marks Establish the Inner Centromere and Chromosome Bi-Orientation, Science (80-.). 330 (2010) 239–243. https://doi.org/10.1126/science.1194498.

[17] P. Wang, X. Hua, Y.H. Bryner, S. Liu, C.B. Gitter, J. Dai, Haspin inhibition delays cell cycle progression through interphase in cancer cells, J. Cell. Physiol. 235 (2020) 4508–4519, https://doi.org/10.1002/jcp.29328.

[18] L. Zhou, C. Liang, Q. Chen, Z. Zhang, B. Zhang, H. Yan, F. Qi, M. Zhang, Q. Yi, Y. Guan, X. Xiang, X. Zhang, S. Ye, F. Wang, The N-Terminal Non-Kinase-Domain-Mediated Binding of Haspin to Pds5B Protects Centromeric Cohesion in Mitosis, Curr. Biol. 27 (2017) 992–1004, https://doi.org/10.1016/j.cub.2017.02.019.

[19] Q. Yi, Q. Chen, C. Liang, H. Yan, Z. Zhang, X. Xiang, M. Zhang, F. Qi, L. Zhou, F. Wang, HP 1 links centromeric heterochromatin to centromere cohesion in mammals, EMBO Rep. 19 (2018) 1–13, https://doi.org/10.15252/embr.201745484.

[20] C. Ghenoiu, M.S. Wheelock, H. Funabiki, Autoinhibition and Polo-Dependent Multisite Phosphorylation Restrict Activity of the Histone H3 Kinase Haspin to Mitosis, Mol. Cell. 52 (2013) 734–745, https://doi.org/10.1016/j.molcel.2013.10.002.

[21] L. Zhou, X. Tian, C. Zhu, F. Wang, J.M. Higgins, Polo-like kinase-1 triggers Histone phosphorylation by Haspin in mitosis, EMBO Rep. 15 (2014) 273–281, https://doi.org/10.1002/embr.201338080.

[22] F. Wang, N.P. Ulyanova, M.S. Van Der Waal, D. Patnaik, S.M.A. Lens, J.M. G. Higgins, A positive feedback loop involving haspin and aurora B promotes CPC accumulation at centromeres in mitosis, Curr. Biol. 21 (2011) 1061–1069, https://doi.org/10.1016/j.cub.2011.05.016.

[23] F. Yu, Y. Jiang, L. Lu, M. Cao, Y. Qiao, X. Liu, D. Liu, T. Van Dyke, F. Wang, X. Yao, J. Guo, Z. Yang, Aurora-A promotes the establishment of spindle assembly checkpoint by priming the Haspin-Aurora-B feedback loop in late G2 phase, Cell Discov. 3 (2017) 1–17, https://doi.org/10.1038/celldisc.2016.49.

[24] J.M.G. Higgins, Haspin-like proteins: A new family of evolutionarily conserved putative eukaryotic protein kinases, Protein Sci. 10 (2001) 1677–1684, https://doi.org/10.1110/ps.49901.

[25] H. Tanaka, Y. Yoshimura, M. Nozaki, K. Yomogida, J. Tsuchida, Y. Tosaka, T. Habu, T. Nakanishi, M. Okada, H. Nojima, Y. Nishimune, Identification and characterization of a haploid germ cell-specific nuclear protein kinase (Haspin) in spermatid nuclei and its effects on somatic cells, J. Biol. Chem. 274 (1999) 17049–17057, https://doi.org/10.1074/jbc.274.24.17049.

[26] P. Wang, X. Hua, Y.H. Li, Y.H. Bryner, R.P. Hsung, J. Dai, Loss of haspin suppresses cancer cell proliferation by interfering with cell cycle progression at multiple stages, FASEB J. 35 (2021) 1–14, https://doi.org/10.1096/fj.202100099R.

[27] J.C. Melms, S. Vallabhaneni, C.E. Mills, C. Yapp, J.-Y. Chen, E. Morelli, P. Waszyk, S. Kumar, D. Deming, N. Moret, S. Rodriguez, K. Subramanian, M. Rogava, A.N. R. Cartwright, A. Luoma, S. Mei, T.J. Brinker, D.M. Miller, A. Spektor, D. Schadendorf, N. Riggi, K.W. Wucherpfennig, P.K. Sorger, B. Izar, Inhibition of Haspin Kinase Promotes Cell-Intrinsic and Extrinsic Antitumor Activity, Cancer Res. 80 (2020) 798–810, https://doi.org/10.1158/0008-5472.CAN-19-2330.

[28] F. Zhang, B. Qiu, Y. Ji, H. Zhang, P. Song, N. Sun, L. Zhao, F. Lv, Y. Lin, Y. Gao, Q. Xue, S. Gao, J. He, Knockdown of GSG2 inhibits the development and progression of non-small cell lung cancer in vitro and in vivo, Cell Cycle 22 (2023) 153–164, https://doi.org/10.1080/15384101.2022.2110441.

[29] Z. Ye, Z. Zhang, L. Fang, D. Tian, X. Liu, Bioinformatic analysis reveals GSG2 as a potential target for breast cancer therapy, Open Life Sci. 14 (2020) 688–698, https://doi.org/10.1515/biol-2019-0078.

[30] W. Yu, W. Liu, Y. Feng, C. Zhu, Knockdown of GSG2 Suppresses the Progression of Colorectal Cancer Cells, Genet. Test. Mol Biomarkers 26 (2022) 26–36, https://doi.org/10.1089/gtmb.2020.0298.

[31] L.I. Bastea, L.M.A. Hollant, H.R. Döppler, E.M. Reid, P. Storz, Sangivamycin and its derivatives inhibit Haspin-Histone H3-survivin signaling and induce pancreatic cancer cell death, Sci. Rep. 9 (2019) 1–10, https://doi.org/10.1038/s41598-019-53223-0.

[32] D. Zhu, X. Gu, Z. Lin, D. Yu, J. Wang, L. Li, HASPIN is involved in the progression of gallbladder carcinoma, Exp. Cell Res. 390 (2020) 111863, https://doi.org/10.1016/j.yexcr.2020.111863.

[33] Y. Chen, D. Fu, H. Zhao, W. Cheng, F. Xu, GSG2 (Haspin) promotes development and progression of bladder cancer through targeting KIF15 (Kinase-12), Aging (Albany. NY). 12 (2020) 8858–8879. https://doi.org/10.18632/aging.103005.

[34] J. Zhou, N.I.E. Wanpin, J. Yuan, Z. Zhang, M.I. Liangliang, C. Wang, R. Huang, GSG2 knockdown suppresses cholangiocarcinoma progression by regulating cell proliferation, apoptosis and migration, Oncol. Rep. 45 (2021) 1–10, https://doi.org/10.3892/or.2021.8042.

[35] L. Li, S. Li, H. Wang, L. Li, P. Wang, D. Shen, X. Dang, GSG2 promotes tumor growth through regulating cell proliferation in hepatocellular carcinoma, Biochem. Biophys. Res. Commun. 625 (2022) 109–115, https://doi.org/10.1016/j.bbrc.2022.07.093.

[36] P. Ghatalia, E.S. Yang, B.N. Lasseigne, R.C. Ramaker, S.J. Cooper, D. Chen, S. Sudarshan, S. Wei, A.S. Guru, A. Zhao, T. Cooper, D.L. Della Manna, G. Naik, R. M. Myers, G. Sonpavde, Kinase Gene Expression Profiling of Metastatic Clear Cell Renal Cell Carcinoma Tissue Identifies Potential New Therapeutic Targets, PLoS One 11 (2016) e0160924.

[37] F. Yu, Y. Lin, X. Xu, W. Liu, D. Tang, X. Zhou, G. Wang, Y. Zheng, A. Xie, Knockdown of GSG2 inhibits prostate cancer progression in vitro and in vivo, Int. J. Oncol. 57 (2020) 139–150, https://doi.org/10.3892/ijo.2020.5043.

[38] Y. Huang, Y. Liu, K. Zhu, X. Ma, R. Lu, M. Zhang, Gsg2 promotes development and predicts poor prognosis of ovarian cancer, Cancer Manag. Res. 13 (2021) 499–508, https://doi.org/10.2147/CMAR.S274807.

[39] A. De Antoni, S. Maffini, S. Knapp, A. Musacchio, S. Santaguida, A small-molecule inhibitor of Haspin alters the kinetochore functions of Aurora B, J. Cell Biol. 199 (2012) 269–284, https://doi.org/10.1083/jcb.201205119.

[40] G.D. Cuny, N.P. Ulyanova, D. Patnaik, J.F. Liu, X. Lin, K. Auerbach, S.S. Ray, J. Xian, M.A. Glicksman, R.L. Stein, J.M.G. Higgins, Structure-activity relationship study of beta-carboline derivatives as haspin kinase inhibitors, Bioorganic Med, Chem. Lett. 22 (2012) 2015–2019, https://doi.org/10.1016/j.bmcl.2012.01.028.

[41] W. Zeinyeh, Y.J. Esvan, B. Josselin, M. Defois, B. Baratte, S. Knapp, A. Chaikuad, F. Anizon, F. Giraud, S. Ruchaud, P. Moreau, Synthesis and biological evaluation of Haspin inhibitors: Kinase inhibitory potency and cellular activity, Eur. J. Med. Chem. 236 (2022) 114369, https://doi.org/10.1016/j.ejmech.2022.114369.

[42] S. Avula, X. Peng, X. Lang, M. Tortorella, B. Josselin, S. Bach, S. Bourg, P. Bonnet, F. Buron, S. Ruchaud, S. Routier, C. Neagoie, Design and biological evaluation of substituted 5,7-dihydro-6H-indolo[2,3-c]quinolin-6-one as novel selective Haspin inhibitors, J. Enzyme Inhib. Med. Chem. 37 (2022) 1632–1650, https://doi.org/10.1080/14756366.2022.2082419.

[43] M.A. Qhobosheane, L.J. Legoabe, B. Josselin, S. Bach, S. Ruchaud, J.P. Petzer, R. M. Beteck, Synthesis and evaluation of 7-azaindole derivatives bearing benzocycloalkanone motifs as protein kinase inhibitors, Bioorganic Med. Chem. 28 (2020) 115468, https://doi.org/10.1016/j.bmc.2020.115468.

[44] K. Kestav, D. Lavogina, G. Raidaru, A. Chaikuad, S. Knapp, A. Uri, Bisubstrate inhibitor approach for targeting mitotic kinase Haspin, Bioconjug. Chem. 26 (2015) 225–234, https://doi.org/10.1021/bc500464r.

[45] M. Schröder, A.N. Bullock, O. Fedorov, F. Bracher, A. Chaikuad, S. Knapp, DFG-1 Residue Controls Inhibitor Binding Mode and Affinity, Providing a Basis for Rational Design of Kinase Inhibitor Selectivity, J. Med. Chem. 63 (2020) 10224–10234, https://doi.org/10.1021/acs.jmedchem.0c00898.

[46] J. Qin, W. Cheng, Y.-T. Duan, H. Yang, Y. Yao, Indazole as a Privileged Scaffold: The Derivatives and their Therapeutic Applications, Anticancer. Agents, Med. Chem. 21 (2021) 839–860, https://doi.org/10.2174/1871520620999200818160350.

[47] J. Elie, O. Feizbakhsh, N. Desban, B. Josselin, B. Baratte, A. Bescond, J. Duez, X. Fant, S. Bach, D. Marie, M. Place, S. Ben Salah, A. Chartier, S. Berteina-Raboin, A. Chaikuad, S. Knapp, F. Carles, P. Bonnet, F. Buron, S. Routier, S. Ruchaud, Design of new disubstituted imidazo[1,2-b]pyridazine derivatives as selective Haspin inhibitors. Synthesis, binding mode and anticancer biological evaluation, J. Enzyme Inhib. Med. Chem. 35 (2020) 1840–1853, https://doi.org/10.1080/14756366.2020.1825408.

[48] A.K. ElHady, D.S. El-Gamil, A.H. Abadi, M. Abdel-Halim, M. Engel, An overview of cdc2-like kinase 1 (Clk1) inhibitors and their therapeutic indications, Med. Res. Rev. 43 (2023) 343–398, https://doi.org/10.1002/med.21928.

[49] R.H. Shoemaker, The NCI60 human tumour cell line anticancer drug screen, Nat. Rev. Cancer. 6 (2006) 813–823, https://doi.org/10.1038/nrc1951.

[50] G. Jerusalem, J. Collignon, H. Schroeder, L. Lousberg, Triple-negative breast cancer: treatment challenges and solutions, Breast Cancer Targets Ther. 8 (2016) 93, https://doi.org/10.2147/BCTT.S69488.

[51] A. Daina, V. Zoete, A BOILED-Egg To Predict Gastrointestinal Absorption and Brain Penetration of Small Molecules, ChemMedChem. (2016) 1117–1121, https://doi.org/10.1002/cmdc.201600182.

[52] C.E. Adkins, R.K. Mittapalli, V.K. Manda, M.I. Nounou, A.S. Mohammad, T. B. Terrell, K.A. Bohn, C. Yasemin, T.R. Grothe, J.A. Lockman, P.R. Lockman, P-glycoprotein mediated efflux limits substrate and drug uptake in a preclinical brain metastases of breast cancer model, Front. Pharmacol. 4 (2013) 1–8, https://doi.org/10.3389/fphar.2013.00136.

[53] M.F. Al-Tawil, S. Daoud, M.M. Hatmal, M.O. Taha, Discovery of new Cdc2-like kinase 4 (CLK4) inhibitors via pharmacophore exploration combined with flexible docking-based ligand/receptor contact fingerprints and machine learning, RSC Adv. 12 (2022) 10686–10700, https://doi.org/10.1039/d2ra00136e.

[54] E. Kang, K. Kim, S.Y. Jeon, J.G. Jung, H.K. Kim, H.B. Lee, W. Han, Targeting CLK4 inhibits the metastasis and progression of breast cancer by inactivating TGF-β pathway, Cancer Gene Ther. 29 (2022) 1168–1180, https://doi.org/10.1038/s41417-021-00419-0.

[55] A.K. Elhady, M. Abdel-Halim, A.H. Abadi, M. Engel, Development of Selective Clk1 and -4 Inhibitors for Cellular Depletion of Cancer-Relevant Proteins, J. Med. Chem. 60 (2017) 5377–5391, https://doi.org/10.1021/acs.jmedchem.6b01915.